Applied Materials Today 37 (2024) 102150

Contents lists available at ScienceDirect

Applied Materials Today

journal homepage: www.elsevier.com/locate/apmt

Polysuccinimide-based nanoparticle: A nanocarrier with drug release delay and zero burst release properties for effective theranostics of cancer

Shehzahdi S. Moonshi [a], Karla X. Vazquez-Prada [a,c,f], Hossein Adelnia [a,c], Nicholas J. Westra van Holthe [c,d], Yuao Wu [a], Joyce Tang [a,b], Andrew C. Bulmer [e], Hang Thu Ta [a,b,*,1,2]

[a] Queensland Micro- and Nanotechnology Centre, Griffith University, Brisbane, Australia
[b] School of Environment and Science, Griffith University, Brisbane, Australia
[c] Australian Institute for Bioengineering and Nanotechnology, University of Queensland, Brisbane, Australia
[d] Centre for Advanced Imaging, University of Queensland, Brisbane, Australia
[e] School of Pharmacy and Medical Sciences, Griffith University, Gold Coast, Australia
[f] Memorial Sloan Kettering Cancer Center, New York, United States

ARTICLE INFO

Keywords:
Nanoparticles
Polysuccinimide
Curcumin
IR-780
Cancer
Photothermal
Photoacoustic imaging
Fluorescence imaging

ABSTRACT

We have developed a novel pH-responsive delivery system consisting of oleylamine-modified polysuccinimide (PSI) nanoparticles (NPs) whereby NPs remained stable and started to release bioactive agents after 8.5 h with maximal release acquired after 36 h under physiological pH. Our NPs did not exhibit any burst release of drug, which is a key advantage in anti-cancer targeted drug delivery system. Here, the NPs function as a carrier for bioactive agents such as Curcumin and IR-780 dye whereby the former exerts its intrinsic anti-cancer abilities, the latter confers photothermal treatment application and bimodal imaging ability using photoacoustic and fluorescence imaging. *In vitro* and *in vivo* results establish that administration of folate receptors targeting PSI-NPs in U87MG model effected in a substantial decrease in tumour and photothermal laser exposure at 808 nm further ablated tumours to an almost total eradication. Our dual loaded targeted NPs demonstrated selectivity through enhanced accumulation and retention in tumours as indicated by multi-spectral optoacoustic tomography (MSOT) and fluorescence imaging (FI). Loading of Curcumin and IR-780 into PSI-NPs improved its bioavailability, allowing Curcumin to be administered into the circulation system and retention in tumours which led to the simultaneous application for a successful targeted, synergistic photothermal treatment and bimodal imaging using MSOT and FI.

1. Introduction

Cancer is the second leading cause of fatality worldwide with 19.3 million new cases and 10 million cancer mortality in 2020 [1,2]. These figures are expected to rise in the future. Hence, intense efforts must be made to develop innovative strategies for effective treatment and diagnosis to prolong patients' life span and quality of life [3–5]. Recently, research focus has shifted towards the utilisation of natural bioactive compounds in anti-cancer application [6,7]. Natural bioactive compounds employed as an anti-cancer strategy include polyphenolic compounds such as Curcumin [8], Quercetin [6] and Resveratrol [7] extracted from *Curcuma longa*, red wine, and chocolate respectively. These natural compounds have been proven effective in many studies focused on their anticarcinogenic properties which includes inhibition of tumor growth, metastasis, and angiogenesis [6,9,10].

Curcumin has displayed several therapeutic benefits such as anti-fungal, anti-bacterial, anti-inflammation, wound healing, anti-cancer and hence been investigated as a treatment agent in various diseases with positive outcomes [10]. In cancer specifically, Curcumin has displayed potent anti-cancer efficacy via targeting and regulating various

* Corresponding author at: School of Environment and Science, and Queensland Micro- and Nanotechnology, Griffith University, Nathan Campus, Brisbane, QLD 4111, Australia.
E-mail address: h.ta@griffith.edu.au (H.T. Ta).
[1] Website: https://hangta.group/
[2] https://experts.griffith.edu.au/27034-hang-ta

https://doi.org/10.1016/j.apmt.2024.102150
Received 16 December 2023; Received in revised form 19 February 2024; Accepted 2 March 2024

signalling pathways resulting in the inhibition of cell proliferation and apoptosis of cancer cells [10,11]. Despite its promising potential, clinical application of Curcumin is impeded by several drawbacks including low aqueous solubility and rapid metabolism which hampers its full therapeutic potential. Consequently, efforts must be dedicated to formulating and delivering Curcumin systemically to improve its bioavailability, accumulation, and retention in tumours whereby the therapeutic benefits can be completely exploited.

Loading such active agents into suitable polymeric carriers are a viable strategy to improve drug solubility and treatment efficacy [12]. Polysuccinimide (PSI) is a water insoluble biocompatible, biodegradable polymer which has been widely adopted for biomedical applications. Synthesis and modification of PSI are highly facile and its degradation yields amino acids or short chain peptide in the body [13]. Consequently, PSI has been utilised in various biomedical purposes such as MRI contrast agent, formulation of plasma expander and drug delivery systems [13]. PSI-based nanocarriers have been developed for the delivery of nucleic acids in anti-cancer treatment strategy [14,15]. Whilst results acquired seemed optimistic, conclusions are drawn based on only *in vitro* evaluations. None of these studies evaluated the *in vivo* efficacy of NPs. Another research group has previously assessed a PEGylated PSI-based nanocarrier conjugated with phenethylamine which was exploited for pH responsive drug release of siRNA for intravaginal delivery in sexually transmitted infections [16]. However, cumulative release behavior displayed a delayed burst release of siRNA after just 1 h at a neutral pH and a significantly lower release at pH 4.2, suggesting stability under acidic conditions. It should be noted that this study did not report any *in vivo* data. Recently, previous study from our group engineered a novel series of PSI polymer particles capable of remaining stable under acidic conditions whilst slowly dissolving under physiological conditions [17]. Here, PSI will function as a carrier of hydrophobic Curcumin, providing a platform for delivery, enhancing their bioavailability, allowing Curcumin to be administered into the circulation, stability, and efficacy hence addressing limitations associated with the clinical application of Curcumin. In this study, PSI was chemically modified to form nanoparticles with delayed dissolution and delayed drug release profiles for a certain period of time, allowing them time to reach the disease sites before disintegrating and releasing the encapsulated cargo.

Theranostics integrates simultaneous therapeutics and imaging to improve drug efficacy and monitor biodistribution and treatment response non-invasively and longitudinally [4,18–22]. Recently, nano-photothermal therapy (NPTT) has emerged as a promising approach based on the utilisation of nanoparticles to convert light to heat upon laser exposure to selectively eliminate cancer cells without ionising radiation. Previous studies have demonstrated the success of NPTT as a non-invasive combinatorial strategy with the inclusion of bioactive therapeutic agents to treat solid tumours effectively [23,24]. Intrinsically, tumours reside in slightly acidic and hypoxic conditions as opposed to non-malignant cells hence cancer cells are more susceptible to heat [25,26]. At an acquired temperature between 43 and 50 °C, apoptosis of cancer cells is induced effecting in the death of cells [27].

IR-780 has demonstrated stability and enhanced fluorescence intensity in comparison to FDA- approved indocyanine green which has been applied in clinical imaging [28]. Benefitting from the optical absorbance in the NIR range (700 to 900 nm), IR-780 dye has exhibited potent efficacy as a theranostic agent in photothermal conversion with minimal invasiveness and high sensitivity in NIR fluorescence *in vivo* imaging [29]. Multi-spectral optoacoustic tomography (MSOT) combines ultrasound and optics which has several advantages including high spatiotemporal resolution and is devoid of ionising radiation [30]. Additionally, NIR fluorescence imaging displayed several benefits such as its high sensitivity, economical and involves non-ionising radiation [31]. As each imaging modality has its inherent pros and cons, combining different imaging tools can overcome limitations involved with a particular equipment [32]. Hence, IR-780 can function as a PTT agent while simultaneously facilitating bimodal MSOT and NIR fluorescence *in vivo* imaging. Despite multiple capabilities, IR-780 is highly lipophilic, has poor aqueous solubility and is eliminated swiftly from the body which hinders its clinical utilisation [33]. Therefore, a localised accumulation and retention at the disease site is required for it to exert its maximal theranostic efficacy, which can be achieved by incorporation into PSI NPs. Hence, PSI permits loading of bioactive agents allowing prolonged circulation, bioavailability and importantly efficacy in the treatment and simultaneous imaging in diseases.

NPs that are decorated with tumour specific targeting ligands can augment NPs uptake, accumulation, and thus therapeutic efficacy thereby minimising adverse effects associated with normal cells. Folic acid (FA), a type of vitamin B complex, has a strong affinity for folate receptors alpha (FRα) based on its over expression in solid tumours including ovarian, breast and brain. Contrastingly, FRα are minimally expressed in normal cells, hence, various reports have established successful targeting of these receptors which resulted in enhanced uptake of NPs and therapeutic outcome in cancer [34–36]. In the present study, for the first time, we developed oleylamine-modified PSI NPs which serves as a carrier for bioactive agents such as Curcumin and IR-780 dye to exert its intrinsic anti-cancer abilities, photothermal treatment application and bimodal imaging ability using PA and fluorescence imaging (Scheme 1). The incorporation of Curcumin and IR-780 into PSI polymer carrier addresses its associated shortcomings by aiming to enhance their bioavailability, circulation, stability, and therapeutic efficacy. Additionally, loaded NPs were functionalised with folic acid (FA-PEG-NH_2) to specifically target highly expressed FRα in cancer cells and the PEG moiety confers stability to these dual loaded NPs [37,38].

The main limitation with polymeric NPs in anti-cancer strategy include the burst release of loaded drugs and low drug loading [39–42]. Whilst the burst release of drug may be employed in certain therapeutic applications such as wound healing [43,44], in anti-cancer treatments, such unpredictable and uncontrolled release is usually undesirable [45]. This is correlated to the safety issues whereby the released drug may exceed the toxicity threshold leading to severe systemic adverse effects [43]. Hence, the development of delayed and sustained release NP systems is crucial to deliver bioactive agents safely and efficiently specifically for cancer treatment. Additionally, delaying the dissolution is crucial specifically in intravenous delivery strategy so that NPs have adequate time for circulation and targeting before they disintegrate [17].

Here, the NPs were programmed with delayed dissolution and delayed drug release profiles, making them stable enough to reach the tumor site before disintegrating and releasing the drugs. Furthermore, burst release, a common limitation of current drug delivery systems and a challenge for translation, was completely absent in our nanosystems.

2. Materials and methods

2.1. Materials

All non-listed chemicals were purchased from commercial suppliers at analytical grade. L-aspartic acid (ASP), sulfolane, phosphoric acid, methanol, sodium hydroxide, dimethyl sulfoxide, N,N-dimethylformamide (DMF), oleylamine (OA), ethylenediamine (EDA), DMF, Curcumin, IR-780 dye, Annexin-V FITC apoptosis detection kit, 2′, 7′-dichlorofluorescin diacetate (DCFDA), Corning® Matrigel® Basement Membrane Matrix were all purchased from Sigma Aldrich and used without further purification. PrestoBlue™ was purchased from Invitrogen™ (Thermo Fisher Scientific). FA-PEG-NH_2 was purchased from Ruixibiotech. Water used in all experiments was deionized water (DI).

2.2. Synthesis of poly(succinimide)

Typical poly-condensation reactions of aspartic acid was adopted to synthesise PSI [17]. In general, aspartic acid (Sigma,14 gr, Mw=133.11

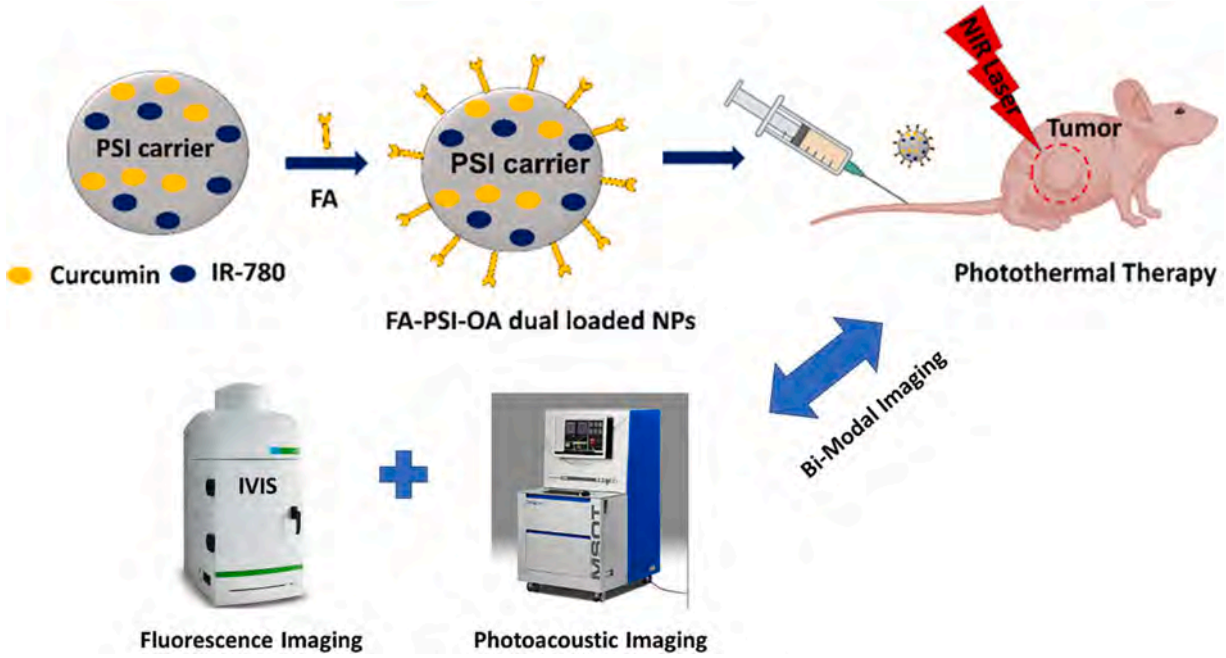

Scheme 1. Schematic illustration of the developed nanoparticles (NPs) platform which comprises of chemically modified oleylamine-Polysuccinimide (PSI-OA) NPs which serve as a carrier for Curcumin and IR-780 dye. Loaded NPs are functionalised with folic acid (FA) ligands for augmented targeting in U87 MG tumor for synergistic photothermal treatment upon laser exposure and bi-modal imaging with fluorescence and photoacoustic imaging.

g/mol, 105.17 mmol), H_3PO_4 (85 wt.% in H_2O, Sigma, 1 mL), and sulfolane (Sigma, 56 mL) were dispensed into a flask placed in an oil bath at 180 °C under nitrogen gas flow with mechanical stirring (150 rpm) [17]. After 5 h, the solution was precipitated in a large amount of deionized (DI) water [17]. The polymer powder (*i.e.*, PSI) was washed several times with DI water to remove excess catalyst and solvent, and finally dried in a freeze drier.

2.3. Synthesis of oleylamine-modified poly(succinimide)

10 mL of 10% w/v of PSI in DMF was mixed with 995 μL of OA and incubated under nitrogen atmosphere at 70 °C for 12 h. The degree of OA modification is 30 % with respect to succinimide units, considering the yield of 100 %. After 12 h, the mixture was cooled, the polymer was washed with methanol to remove un-reacted OA as well as excess DMF, and finally the polymer was freeze-dried [46].

2.4. Synthesis of dual loaded Curcumin and IR-780 PSI-OA nanoparticles by emulsion evaporation method

10 mg/mL of Curcumin and IR-780 respectively were prepared in 1 mL of DCM. 50 μL (10 mg/mL stock) each of Curcumin and IR-780 respectively, 500 μL of polymer solution (40 mg/mL PSI-OA stock solution in DCM), 400 μL of DCM and 2 μL of DMSO were added into a new tube to make 1 mL total volume of polymer mixture which equates to a final concentration of 500 μg/mL of Curcumin and IR-780 each.

Then, 10 mL of partially hydrolysed PVA solution (2.5 wt.%) was added to the polymer mixture and solution was sonicated for 2 min (Amplitude 50 %, Pulse: 2 s on-2 s off). After sonication, the emulsion was placed at room temperature overnight to allow evaporation of DCM using the highest stirring speed with a magnetic bar of size 1 cm. Subsequently, the NPs were washed twice with DI water by centrifugation at 92 600 g rpm for 1 h to remove PVA, and the NPs were re-dispersed in water by pipetting. The theoretical final concentration of Curcumin and IR-780 dye was 500 μg/mL each.

2.5. Conjugation of Folic-PEG-NH_2 to PSI-OA NPs

The conjugation of FA-PEG-NH_2 was conducted with a mass ratio of 1:10 of FA to NPs. The final concentration of NPs in the reaction was 2 mg/mL. The reactions were carried out for 4 h at room temperature in DI water without the use of any catalysts followed by twice washing with DI water (separation with centrifugation at 92 600 g for 30 min, re-dispersion with pipetting). After washing, the zeta potential, and the size of the particles were measured.

2.6. Characterisation of NPs

Dynamic light scattering (DLS) (Zetasizer Nano ZS) was employed to determine the size and zeta potential of the NPs [47,48]. Transmission electron microscopy (TEM) [49] images were taken on a JEOL-JEM-1010 TEM, operating at an accelerating voltage of 80 kV. ATR-FTIR (Nicolet 5700 FT-IR) was also used to analyze the changes in surface groups of the PSI-OA NPs. The spectra were the average of 16 scans captured in the wavenumber range of 4000–400 cm^{-1}. The absorption of the nanoparticles was determined using a Clariostar UV–vis spectrophotometer for a wavelength range between 300 and 1000 nm [50].

2.7. Encapsulation efficiency

Curcumin and IR-780 standards were prepared using similar methodology adopted to synthesise nanoparticles as described above. The supernatant of the NPs after the centrifugation step was collected prior to nanoparticle resuspension to measure the encapsulation efficiency (EE) of Curcumin and IR-780 in the NPs. The standard curve was used to determine the EE of Curcumin and IR-780 in the NPs based on the absorbance of the supernatant using the following Equation [51] 1 and 2:

$$EE = \frac{[Cur]added - [Cur]supernatant}{[Cur]added} \; X \; 100\% \quad (1)$$

$$EE = \frac{[IR-780]added - [IR-780]supernatant}{[IR-780]added} \; X \; 100\% \quad (2)$$

2.8. Dissolution of PSI-OA NPs

The dissolution of the PSI-OA NPs was assessed under different pH conditions (4.5, 6.5, 7.4 and 8). 50 μL (2 mg/mL) was added to the respective buffers (150 μL) with different pH values (4.5, 7.4, 8). The final concentration of NPs in each well was 500 μg/mL. The mixture was transferred to a 96-well plate and placed in microplate reader operating at 37 °C. The absorbance values were measured at 350 nm over time [17].

2.9. Release of Curcumin and IR-780 from PSI-OA NPs

The experiment setup was similar to the dissolution assay above with the addition of 0.2% of Tween 20 in the respective buffers to aid in the release of Curcumin and IR-780. Absorbance of the dispersions in different pH conditions at 37 °C were measured at 425 and 780 nm for every 15 min. Shaking at 100 rpm on a 50 mm orbital diameter was performed prior to absorbance measurement. As the PSI-OA NPs also demonstrate an absorbance at 425 and 780, the changes in absorbances are due to both particle dissolution and Curcumin and IR-780 release. Therefore, the release was calculated following equations [52] 3 and 4:

$$Curcumin\ release\ (\%) = \frac{425nm\ (cur) - 425nm(unloaded)}{425nm\ (cur)} x100\% \quad (3)$$

$$IR-780\ release\ (\%) = \frac{780nm\ (dye) - 780nm(unloaded)}{780nm\ (dye)} x100\% \quad (4)$$

2.10. Photothermal ability of NPs

In a 96-well plate, photothermal effects of NPs in solution were evaluated based on the increment in temperature of different concentrations of IR-780 upon laser exposure at 808 nm under varying laser power. Thermographic images and temperature were noted using a thermal camera [52].

2.11. Phantom photoacoustic imaging (PAI)

All photoacoustic experiments were performed with a pre-clinical MSOT inVision 256 (iThera Medical, Munich, Germany) with a 270° array of transducer detector elements and a central ultrasound frequency of 5 MHz. Laser radiation was generated from a Q-switched Nd:YAG laser with a pulse duration of 8 ns and a repetition of 10 Hz. Photoacoustic (PA) data processing and quantification were performed using ViewMSOT 4.0 software suite (iThera Medical) with phantom images reconstructed using a back-projection algorithm. PA spectroscopy was acquired at 25 °C between 680 – 980 nm with a step size of 5 nm, using 3 averages per wavelength. PA spectroscopy measurements were obtained over a section of the phantom vessel with a step size of 0.5 mm. PA signal intensity was recorded as the mean pixel intensity of a region of interest (ROI) drawn within the internal diameter of the phantom, excluding the phantom vessel wall thickness. The PA spectrum was averaged over the scan range and recorded spectra are displayed as the averaged signal over the phantom vessel scan range.

2.12. In vitro studies

2.12.1. Cell culture of cancer cells

Human glioma cancer cells (U87-MG), and Chinese hamster ovarian (CHO) cells were purchased from the American Type Culture Collection (ATCC, Manassas, VA). Cells were cultured in Dulbecco's modified Eagle medium (DMEM, Invitrogen), supplemented with 10 % fetal bovine serum, 100 U/mL penicillin and 100 μg/mL streptomycin, at 37 °C in a humidified atmosphere, with 5 % of CO_2 [3, 53].

2.12.2. Targeting study

A panel of cancer cell lines from various sources such as the brain, breast, skin and ovary (MDA-MB-231, B16F10, MCF-7, Skov-3 and U87MG) that were available in the lab were screened looking at both NP uptake with and without folic acid targeting via fluorescence intensities and cytotoxicity using PrestoBlue assay. Briefly, cells were seeded at a density of 8×10^3 per well, in 100 μL of cell culture medium, and incubated for 24 h to allow cell adherence. Cells were incubated for 1 h with PSI-OA loaded with IR-780 dye with and without FA targeting ligand. Cells were washed with PBS thrice and fluorescence intensity was measured using Sapphire imaging. Cells were seeded onto coverslips and PSI-OA dual loaded NPs was added and incubated for 1 h. The cells were fixed for 20 min in 4 % paraformaldehyde (PFA), before being rinsed 3 × 5 min in phosphate-buffered saline (PBS). Cover slips were mounted with DAPI in Vectashield on glass slides and imaged using the Olympus microscope [54].

2.12.3. Haemocompatibility assay

This experiment was performed under human ethics (2021/598) approved by Griffith University human thics committee. Informed written consent from all participants was obtained prior to the research. Blood was drawn from healthy volunteers in 3.2 % sodium citrate containing vials. All the experiments were performed within 3 h of collection. Experiments were performed in triplicate. PBS (pH=7.4) and 1 % Triton X-100 served as negative and positive controls, respectively. For the haemolysis assay [55], red blood cells were obtained by centrifugation of whole blood at 161 g for 15 min. The pellet was washed twice and resuspended (1:50) with PBS (pH=7.4). Immediately, 180 μL of the solution was incubated at 37 °C with increasing concentrations of NPs (20 μL) and mild shaking. The incubated red blood cells were then centrifuged (161 g for 15 min) and the supernatant was collected. Absorbance was measured at 545 nm using a microplate reader (FLUOstar Omega microplate reader, BMG LABTECH). Plasma haemoglobin was estimated to calculate the percentage of haemolysis by the following equation:

Haemolysis (%) = (OD sample- OD negative control) / (OD positive control-OD negative control) x 100

2.12.4. Cytotoxicity assay

Cells were seeded into 96-well plates at cell densities of 10,000 cells/well and allowed to attach overnight. Cells were treated with different concentrations of NPs for 24 h. For laser groups, media was replaced with fresh media and cells were irradiated with an 808 nm infrared laser (light intensity= 1.5 W/cm^2, laser-diameter= 2 cm) for 5 min in a custom build stabilized infrared fibre laser system (MDL-II-808 laser, EFORCE AUSTRALIA PTY LTD). Temperature was recorded using a thermal camera (FLIR CX-Series) [56]. After treatment, cells were incubated with 1× PrestoBlue® cell viability reagent for 30 min at 37 °C and 5% CO^2. Metabolically active cells can reduce the PrestoBlue reagent, with the fluorescence changes used as an indicator to quantify the viability of cells in culture. Cell viability was measured according to the manufacturer's instructions. Viable cells were detected by fluorescence intensity measurement using CLARIOstar® Plus plate reader (BMG Labtech) at 560/590 nm (excitation/emission). The fluorescence of non-treated cells was determined as 100% cell viability [57].

2.12.5. Cell apoptosis assay

Annexin V-FITC assay was utilized to assess apoptosis of U87-MG cells (1×10^5 cells/well) in 24 well plates. After 24 h, cells were treated with 100 μg/mL of NPs for 24 h. For the laser group, cells were further exposed to laser at 1.5 W/cm^2 for 5 min. For flow analysis, all attached and floating cells were collected and washed thrice with PBS. Cells were suspended in binding buffer, stained with Annexin V-FITC

and propidium iodide (PI) for 15 min in the dark [58]. Stained cells were analysed using the Accuri6 cytometer and Flowjo software.

2.13. In vivo study

2.13.1. Animal study

Animal studies were conducted at the Centre of Advanced Imaging (CAI), University of Queensland (St Lucia, Brisbane), in accordance with the national guidelines provided and approved by the institutional animal care and ethics committees of the University of Queensland (# 2021/AE000423). All animals were sourced from Animal Resources Centre (Murdoch, Perth) and acclimatised for full seven days at CAI animal holding room prior to commencement of experiments. Procedures including tumour induction, treatment administration, MSOT, fluorescence imaging and terminal blood collection were performed on mice placed under isoflurane anaesthesia (1–4% isoflurane with an air-oxygen mixture at a flow rate of 400 mL/min). Throughout the experiment period, animals were monitored for signs of distress or ill health with appropriate husbandry and supportive therapies including deep and clean supportive bedding, warm, quiet and dim environment, fluids and food and water in a palatable readily available form provided.

2.13.2. Biosafety assessment

10-week-old female C57BL/6 J mice were randomly divided into three groups and administered with saline ($n = 4$), (3.7 mg/kg Curcumin, 200 mg/kg NPs, $n = 4$) and (7.3 mg/kg Curcumin, 400 mg/kg NPs, $n = 4$) via intravenous (IV) tail vein injection on days 0, 4 and 8 to assess the biocompatibility of NPs. Mice were monitored every 2 days for changes in body weight. At day 12, mice were placed under deep anaesthesia and 600–800 μL of blood were collected from each mouse by cardiac puncture. The whole blood was left undisturbed at room temperature for 30 min to allow clotting, then centrifuged at 4000 g for 30 min at 4 °C. The resulting supernatant (serum) was collected immediately and stored at −20 °C for further biochemical analysis. Clinical chemistry analysis of serum (glucose, bilirubin, albumin, alanine transaminase, creatinine, urea and uric acid) was completed on a Beckman Coulter AU480 analyser (Lane Cove, Australia) [59]. Frozen aliquots were thawed, centrifuged at 21,500 g for 10 min (room temperature) prior to analysis. All analyses were conducted after the instrument passed calibration (system check) and quality control. Samples were analysed in single or duplicate, with duplicate measures averaged. Data were compared to reference ranges for rodents per published results [60,61]. After blood collection, major organs including heart, lung, liver, spleen and kidney were harvested for weighing and then stored in 4% PFA solution, sliced and stained with hematoxylin and eosin (H&E) for histological analysis [62].

2.13.3. Efficacy

To establish tumour models, 10-week-old female BALB/c nude mice were each subcutaneously injected with 100 μL U-87 MG cells (7.5×10^6 cells suspended in 1:1 ratio of Matrigel® Basement Membrane Matrix and L-15 medium) into the right flank. The tumour size was monitored every other day using a digital vernier calliper, and the tumour volume (V) was calculated using the formula: $V = (\text{Length} \times \text{Width}^2)/2$ [63]. When tumour volume reached 100 - 150 mm^3, mice were randomly divided into four groups ($n = 5$) and intravenously injected through tail vein with 100 μL saline, NPs (0.9 mg/kg of Curcumin and 0.9 mg/kg of IR-780), FA-NPs (0.9 mg/kg of Curcumin and 0.9 mg/kg of IR-780) and FA-NPs (0.9 mg/kg of Curcumin and 0.9 mg/kg of IR-780) + laser irradiation. The anti-cancer efficacies of the treatment groups were assessed by monitoring tumour volume and body weight every 2 days. Mice from laser groups were exposed to an 808 nm infrared laser (light intensity= 1.5 W/cm^2, laser-diameter= 1 cm) for 5 min in a custom build stabilized infrared fibre laser system (MDL-II-808 laser, EFORCE AUSTRALIA PTY LTD). Temperature was recorded using a thermal camera (FLIR CX-Series). At the end of the experiment, mice were sacrificed, and tumours were weighed and harvested [48]. TUNEL assay of tumours was performed using a kit (ab206386) as per manufacturer's instructions.

2.13.4. Targeting efficacy using MSOT and fluorescence imaging

2.13.4.1. MSOT photoacoustic imaging. *In vivo* photoacoustic experiments were performed with a pre-clinical MSOT inVision 256-TF imaging system (iThera Medical, Munich, Germany). Whole-body imaging was performed on anaesthetised U-87 MG tumour-bearing mice at 0, 24 h, 48 h post tail vein injection with PSI-NPs (0.9 mg/kg of Curcumin and 0.9 mg/kg of IR-780) and FA-NPs (0.9 mg/kg of Curcumin and 0.9 mg/kg of IR-780). Anaesthetised mice were positioned in a supine position within the animal holding frame with 2 % isoflurane and a O_2 flow rate of 0.4 L/min, coated with ultrasound coupling gel, and wrapped in a thin polyethylene membrane. Air pockets were removed from the vicinity of the tumour volume. Mice were submerged within the 37 °C imaging chamber and positioned within the 270° ultrasound transducer array with the scan range defined to correspond with the tumour position. Mice were z-translated through the imaging plane in 0.3 mm steps to acquire a stack of 2D axial images over the scan region. 10 frames per wavelength at 680, 700, 730, 760, 790, 820, 850, 900, and 950 nm were acquired. Images were reconstructed with a model-based algorithm and processed using a linear spectral-unmixing algorithm to identify the signal of oxy-haemoglobin (HbO2), haemoglobin (Hb) and the NPs. PSI-OA NP PA spectrum was input into the unmixing algorithm to identify image pixels associated with the PSI-OA NPs. A fluence correction algorithm was applied to the MSOT images post reconstruction. A region of interested (ROI) of consistent dimensions was defined in the XY plane of each image frame set at the centre of the tumour volume for quantitative analysis [56].

2.13.4.2. IVIS fluorescence imaging. The biodistribution of the NPs was monitored real-time using an *in vivo* fluorescence imaging system IVIS Lumina X5. Whole-body imaging was performed on anaesthetised U-87 MG tumour-bearing mice at 0, 30 min, 24 h, 48 h and 6 days post tail vein injection with PSI-NPs (0.9 mg/kg of Curcumin and 0.9 mg/kg of IR-780) and FA-NPs (0.9 mg/kg of Curcumin and 0.9 mg/kg of IR-780). Fluorescence intensities were determined using the ROI function of Aura Imaging Software (Spectral Instruments Imaging).

2.14. Statistical analysis

Data are presented as mean ± standard deviation. One-way ANOVA and student *t*-test were employed for significance testing with p value $\leq$ 0.05 considered statistically significant. Data analyses were performed using GraphPad Prism (GraphPad Software Inc.)

3. Results and discussion

3.1. Characterisation of PSI-OA, dual loaded and FA conjugation NPs

Synthesis via precipitation method, characterization and dissolution of PSI NPs have already been presented in our previous paper where colloidally stable NPs within the size range of 150–500 nm were obtained, however, loading of hydrophobic agents via this technique is problematic and yielded a low loading capacity [17]. Hence, the emulsion strategy was utilised for the loading of hydrophobic bioactive agents and discussed further in this paper. PSI was modified with oleyl amine as established in our previous study and pure PSI-OA NPs were prepared via emulsion evaporation method which yielded a size of 181.0 nm, a low PDI of 0.135 and negatively charged surface at −29.8 mV (Table S1). The functional groups at the end of the polymer chains (*i.e.* aspartic acid) or partial hydrolysis of succinimide groups on the surface of the NPs resulting in aspartic acid contributing to the negative charges

of this NPs. Parameters including solvent, evaporation temperature, and emulsifiers were assessed to obtain an optimised protocol which included the utilisation of partially hydrolysed PVA as colloidal stabilizer, DCM as the solvent for the polymer and room temperature evaporation of the solvent. The latter was particularly significant as increased temperature led to foam formation, DCM boiling, and consequently emulsion destablization. Curcumin, a natural polyphenolic compound, has been established as a promising therapeutic strategy in a variety of diseases including cancer. Nonetheless, its clinical application is hindered by several drawbacks including low aqueous solubility and rapid metabolism [64]. Hence, Curcumin loading into PSI-OA NPs not only addresses these limitations but it also enables targeting to the disease site. IR-780 dye has exhibited potent efficacy in photothermal therapy, however, a localised accumulation at the disease site is required for it to exert a therapeutic effect, which can be achieved by incorporation into PSI-OA NPs [65]. Curcumin and IR-780 dye were incorporated into PSI-OA carrier, enhancing their bioavailability, circulation, stability, and efficacy. Curcumin and IR-780 loaded PSI-OA NPs (dual-loaded) displayed an average hydrodynamic diameter of 211.1 nm, with a narrow PDI of 0.149 and an enhanced negative charge at −35.6 (Table S1 and Fig. 1B).

These NPs allow facile conjugation with various amine containing molecules based on the presence of highly reactive succinimide groups on the surface of the NPs. Consequently, succinimide can react with amine at room temperature without the presence of catalyst. Naïve NPs can be recognised and cleared from the circulation efficiently through the reticuloendothelial system which then impedes its homing ability to tumour [37]. Consequently, the addition of PEG confers reduced immunogenicity, enhanced stability and improves the half-life of NPs in circulation by evading immune surveillance [37]. Additionally, FRα targeting allows effective anti-cancer application of NPs based on established studies displaying improved uptake of targeted NPs in contrast to non targeted NPs [34,35]. FA binds strongly to FRα receptors that are overtly expressed in cancer cells and enters cells through endocytic pathways. Subsequently, FRα moietiesare recycled back to the cell surface [66]. Therefore, PSI-OA NPs loaded with Curcumin and IR-780 were conjugated with FA-PEG-NH_2 to primarily target FRα that are over expressed in cancer cells, thereby enhancing delivery, localisation, stability and therapeutic efficacy of NPs in U87-MG mice model. At FA-PEG-NH_2: PSI-OA NPs ratios higher than 1:10 (Table S2), NPs had a larger size and PDI which suggests aggregation and lack of stability of NPs. A mass ratio of 1:10 of FA:NPs was selected as the optimised parameter based on the size and PDI of the NPs (Table S2). As depicted in Fig. 1D, E, the presence of the characteristic peak of PEG on the conjugated NPs (peak at 1088 cm^{-1}) was obseved in the ATR-FTIR. Size of the NPs increased to 220.0 nm with a low PDI of 0.181 and zeta potential decreased from −35.6 to −20.6 mV (Fig. 1B, C and Table S1) suggesting effective conjugation of FA targeting ligand. TEM images corroborated the size and uniformity of FA conjugated dual loaded PSI-OA NPs (Fig. 1A). It is important to mention that the NPs appear agglomerated in TEM image. It is common due to the drying effect when we prepared the NPs on copper grid for TEM. The NPs were actually not agglometated as evidenced by its low PDI (below 0.2, Table S1). Evidently, Uv-Vis spectra of dual loaded NPs displayed 2 distinct peaks centred at 425 and 800 nm wavelength which corresponds to Curcumin and IR-780 respectively (Fig. 1F).

3.2. Stability, encapsulation efficiency, release of bioactive agents, photothermal and PAI efficacy of NPs

3.2.1. Dissolution of PSI-OA NPs

The dissolution of the dual loaded PSI-OA NPs was assessed in different pH buffers at 37 °C [17]. The dissolution of the NPs is indicated by a decrease in the absorbance of the particles. Accordingly, the dissolution of the NPs results from the hydrolysis of succinimide groups (hydrophobic) by hydroxide ions (OH-), resulting in the formation of water-soluble aspartic acid residues in the polymer structure. Constant normalized absorbance at around 1 represents colloidal stability of NPs over time. NPs remained stable at a slightly acidic pH of 4.5 due to the low levels of OH- (Fig. 2A). Dissolution of dual loaded PSI-OA NPs was evaluated at pH 6.5 to mimic the tumour microenvironment which is between pH 6.5–6.8. At pH 6.5 and 7.4, the NPs remained stable for 8.5 h before starting to disintegrate in the buffer and total dissolution was acquired in 36 h for the latter. For the former, NPs disintegrated

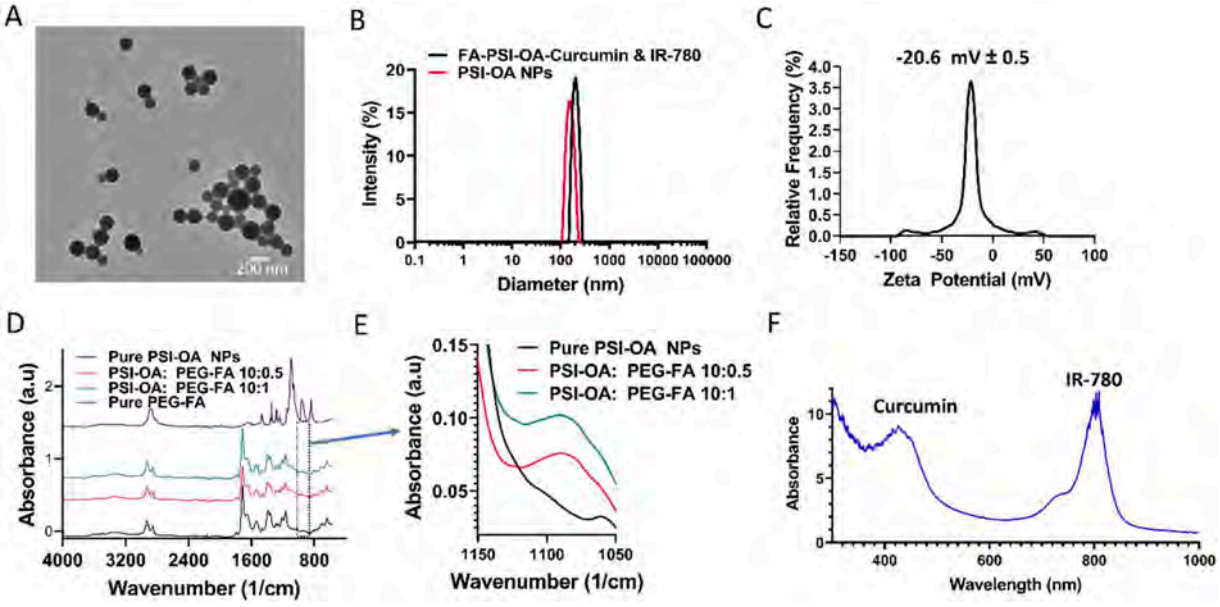

Fig. 1. Characterization of PSI-OA NPs. (A) TEM images showing dual loaded PSI-OA NPs conjugated with FA. (B) DLS data demonstrating the size intensity (%) distribution of the empty PSI-OA NPs and complete dual loaded with FA conjugated PSI-OA NPs. (C) Zeta potential of complete FA conjugated dual loaded PSI-OA NPs. (D) ATR-FTIR spectra of pure PSI-OA NP, pure PEG-FA, and conjugated particles at different ratios of 10:0.5, and 10:1. The characteristic peak of PEG is at 1088cm^{-1}, which is seen in the conjugated NPs (E) when the spectra are magnified. (F) Absorbance of dual loaded PSI-OA NPs in water depicts 2 peaks at 440 and 800 nm representing Curcumin and IR-780 dye respectively.

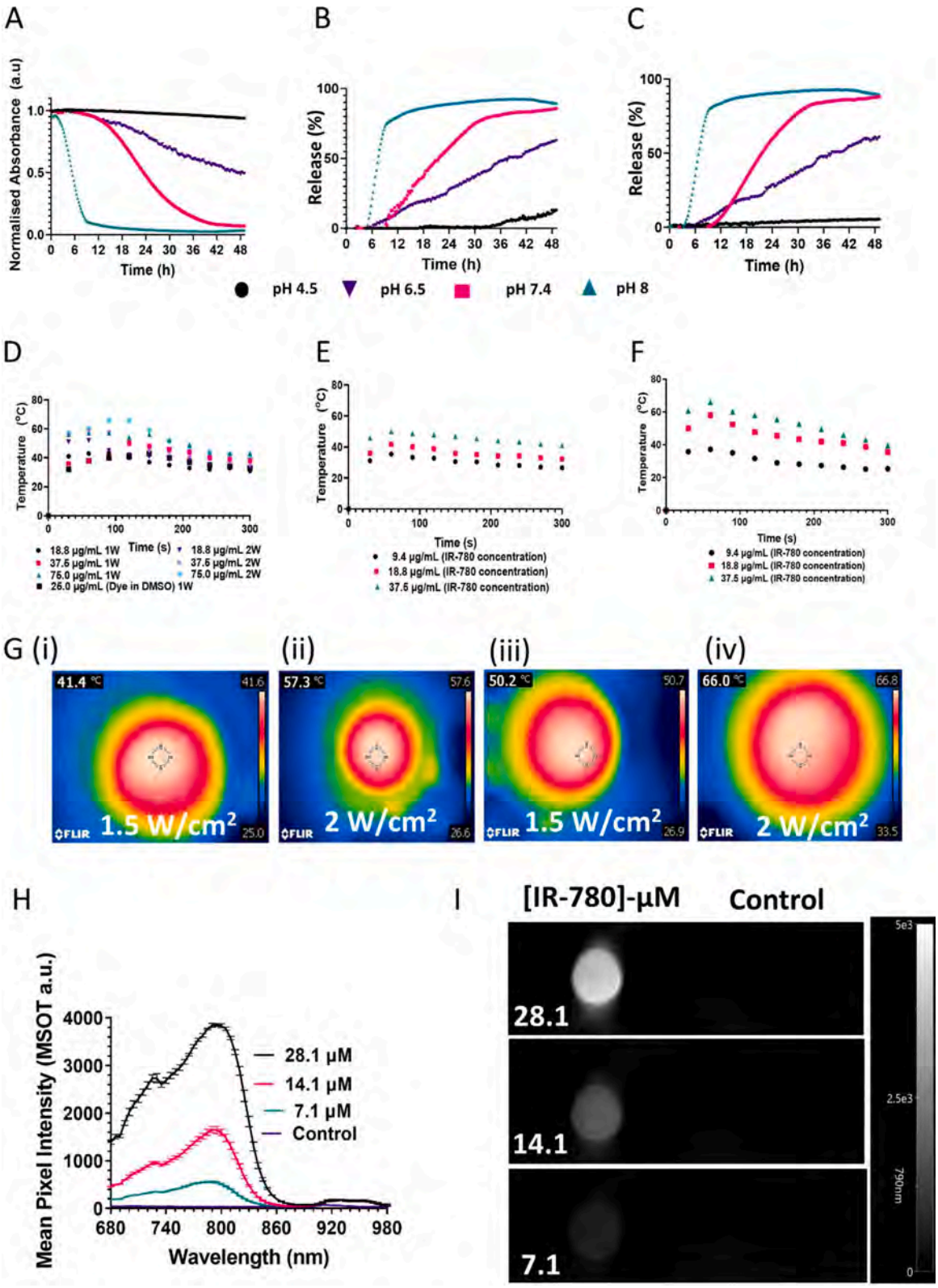

Fig. 2. Properties of NPs. A-C) Dissolution of PSI-OA NPs. (A) Normalized absorbance (at 320 nm) of PSI-OA NPs at 37 °C as a function of time at different pH conditions of 4.5, 6.5, 7.4 and 8. Release of (B) IR-780 and (C) Curcumin from dual-loaded PSI-OA NPs at 37 °C at different pH conditions of 4.5, 7.4, and 8. The release buffer contained 0.2% Tween-80. Photothermal temperature elevation of PSI-OA loaded with (D) IR-780 only and (E, F) with Curcumin and IR-780. The solutions with different concentrations of NPs were irradiated with NIR laser for 5 min at different power densities of W/cm^2: (E) 1.5 W/cm^2 and (F) 2 W/cm^2. (G) The corresponding NIR thermographic images of the wells at the 60th second, containing dual loaded NPs with 18.8 µg/mL IR-780 at (i) 1.5 and (ii) 2 W/cm^2 respectively and with 37.5 µg/mL at (iii) 1.5 and (iv) 2 W/cm^2 respectively. (H) Photoacoustic spectrum of dual-loaded PSI-OA NPs phantoms showing an increase in signal intensity with increasing IR-780 concentration. Control is water. (I) PA images of phantom tube cross-section at 790 nm with dual-loaded PSI-OA NPs showing increased amplitude with increasing concentration of IR-780. Water is used as control.

gradually and did not acquire total dissolution at 48 h timepoint. The modification of PSI with the highly hydrophobic oleylamine prevents water diffusion thus delaying the initiation of dissolution, thereby leading to relative stability of the NPs for 8.5 h. The delayed dissolution and stability of NPs for 8.5 h at physiological pH is crucial specifically in intravenous delivery strategy so that NPs can protect its cargo from premature release or degradation and have adequate time for circulation, targeting and accumulation in the tumour before they disintegrate and release the bioactive agents. At pH 8, NPs disintegrated more rapidly and totally dissolved in 18 h (Fig. 2A). Additionally, the obtained results whereby PSI-based NPs remained stable under acidic condition, while gradually disintegrating in neutral environment, represents a highly desirable feature for drug delivery systems. Considering this significant attribute, PSI based NPs can be exploited not only for systemic, but also for oral delivery in the treatment of various diseases. The acquired results demonstrated successful tuning of the dissolution rate of PSI-NPs via chemical modification which confers stability of PSI-NPs under acidic conditions and its ability to dissolve gradually at pH 7.4, releasing its cargo. In the context of oral delivery, owing to the stability at acidic pH conditions, PSI-NPs can protect the cargo from release or degradation and remain stable in the harsh environment in the stomach [67]. However, after passing through the stomach, as the pH increases, the particles slowly dissolve and release the loaded bioactive agent in the colon. Hence, due to this intrinsic dissolution characteristic, PSI-based NPs can be utilised as a carrier for the oral delivery of chemotherapeutic drugs to the colon for the treatment of colon cancer. PSI-based NPs presents itself as a promising candidate to function as a carrier of bioactive agents via oral delivery and a potential alternative for commercially available Eudragit which is non-biodegradable, invokes side effects related to gastrointestinal complications and is extremely difficult to be modified for targeting purposes [68].

3.2.2. Encapsulation efficiency & release

The encapsulation efficiency of Curcumin and IR-780 in PSI-OA NPs were in the range of 73% ±1.35 and 75 % ± 0.9 respectively. The release of Curcumin and IR-780 was assessed based on the measured absorbance via the UV–Vis spectrophotometer of the samples at 320, 425 and 780 nm in different pH conditions at 37 °C for 48 h with every 15 min (Fig. 2B& C). 0.2 % Tween 20 was added to aid the solubility of Curcumin in the buffer. A decrease in absorbance at 320 nm represents the dissolution of the polymer only as Curcumin and IR-780 have no absorbance at that wavelength. A decrease in absorbance at 425 nm and 780 nm represents particle dissolution and release of Curcumin and IR-780 respectively. The release of IR-780 at pH 4.5 was very slow and reached 13 % after 49 h (Fig. 2B). At pH 6.5, IR-780 was released gradually whereby 50 % and 62.8 % release was acquired at 38 h and 48 h respectively. Contrastingly, at pH 8, IR-780 was released more rapidly whereby 50% release was attained in 7.5 h (Fig. 2B). At pH 7.4, release of IR-780 occurred only after 9.25 h, reached 50% after 22 h and a plateau (maximal release) was achieved at 36 h timepoint which corroborates with the dissolution profile of the NPs (Fig. 2A). Similarly, the release of Curcumin at pH 4.5 was extremely slow and only reached 5 % after 49 h (Fig. 2C). Likewise, at pH 6.5, Curcumin was released slowly whereby 50 % and 60.8 % release were only attained after 38 h and 48 h timepoint respectively. The gradual release of Curcumin and IR-780 at pH 6.5 is ideal for the application of NPs in the treatment of tumour whereby the tumour microenvironment is generally slightly acidic at pH 6.5–6.8. Correspondingly, at pH 7.4, Curcumin was released after 9.5 h, reached 50 % after 22 h and maximal release was acquired in 36 h. The release of Curcumin and IR-780 occurred after 8.5 h which clearly correlates with the dissolution rate of NPs (Fig. 2A). Polysuccinimide-based nanocarriers have been developed for the delivery of nucleic acids in anti-cancer treatment strategy [14,15]. Whilst results acquired seemed optimistic, conclusions are drawn based on *in vitro* evaluations. None of these studies evaluated the *in vivo* efficacy of NPs. Another research group has previously assessed a PEGylated PSI-based nanocarrier conjugated with phenethylamine which was exploited for pH responsive drug release of siRNA for the intended purpose of intravaginal delivery in sexually transmitted infections [16]. However, cumulative release behavior displayed a delayed burst release of siRNA after just 1 h at a neutral pH and a significantly lower release at pH 4.2. It should be noted that this study did not report any *in vivo* data.

At pH 8, similar to IR-780 release, 50% of Curcumin was released in 7.25 h. The release of cargo from nanoparticles can occur through a combination of passive diffusion and degradation/erosion of the NPs. Overall, based on the dissolution/release data, Curcumin and IR-780 were released at similar rates due to degradation/erosion type diffusion rather than passive diffusion type owing to the hydrophobicity of Curcumin and IR-780. Thus the data attained substantiates the dissolution profile of the NPs in different pH buffers. Interestingly, burst release of Curcumin and IR-780 was not observed with our nanoparticles. In anti-cancer application, delaying the beginning of dissolution process is essential specifically in intravenous delivery strategy so that NPs have adequate time for circulation and targeting before they disintegrate. Previously reported study from our group has explored various strategies to delay dissolution of PSI-NPs whereby PSI were modified with ethylenediamine and oleylamine (OA) and the initial dissolution was delayed by 4 and 12 h respectively [17]. Hence, this study confirmed that PSI without modification resulted in immediate dissolution of NPs which equates to burst release of cargo. Additionally, the overall dissolution was also significantly extended in the case of OA modification to around 36 h [17]. The delayed dissolution can be accredited to the incomplete network formation by EDA in the former, and the increased hydrophobicity as well as lower water diffusion in the latter. Hence, in this anti-cancer application, PSI was modified with oleylamine.

3.2.3. Photothermal effects of NPs

Photothermal effects of IR-780 loaded and dual loaded PSI-OA NPs were evaluated based on the increment in temperature of different concentrations of IR-780 upon laser exposure at 808 nm under varying laser power. Thermographic images and temperature were noted using a thermal camera. At 18.8 μg/mL of PSI-OA-IR-780, temperature rose to 43 °C at 1 W/cm^2 and 52 °C at a higher laser strength of 2 W/cm^2 after 60 s. Similarly, 50 and 100 μg/mL of PSI-OA-IR-780 resulted in a further increase in temperature corresponding to the increased NP concentration and laser power (Fig. 2D). Interestingly, 25 μg/mL of IR-780 dye in DMSO at 1 W/cm^2 resulted in a temperature increase to a maximum of 43 °C after 150 s whilst temperature reached 43 °C more rapidly in 60 s with IR-780 loaded NPs. Dual loaded NPs demonstrated a maximal temperature at 60 s after laser exposure, after which temperature declined till the 300th second (Fig. 2E). Upon laser irradiation at 1.5 W/cm^2, 9.1 μg/mL (IR-780 concentration) resulted in a temperature average of 35.5 °C at the 60th second. At higher concentrations of 18.8 and 37.5 μg/mL (IR-780 concentration), temperature increased further to an average of 41.7 °C and 50 °C respectively (Fig. 2D). Correspondingly, a higher laser power of 2 W/cm^2 (Fig. 2F) effected in a substantial increase in temperature of an average of 37.2 °C, 58.0 °C and 65.9 °C with increasing IR-780 concentrations (9.1, 18.8 and 37.5 μg/mL). In contrast, temperature increase of PBS was insignificant. These data exhibited that the NIR-heating effect of NPs were dependent on the IR-780 concentration, laser strength and period of time of laser irradiation. Notably, single loaded IR-780 and dual loaded PSI-OA NPs could effectively convert NIR light to generate heat resulting in temperature elevation hence functioned as a photothermal agent for tumour ablation. Importantly, the addition of Curcumin did not negate the photothermal effects of IR-780 in the NPs. Fig. 2G illustrates the representative thermographic images of dual loaded NPs at the 60th second. A high photothermal conversion efficiency is a critical factor to assess the potential application of NPs in laser induced photothermal therapy. Here, it was calculated to be 31.5% (Fig. S1). Whilst the photothermal conversion efficiency acquired here is lower in comparison to other published

studies on IR-780 loaded NPs in anti-cancer application (40 - 60%) [69–71], it should be noted that the anti-cancer abilities of our NPs are conferred by the synergistic exploitation of the inherent Curcumin activity and the photothermal treatment application via the IR-780 dye. Additionally, our photothermal conversion efficiency attained here is comparable or better than other nanomaterials previously exploited as a photothermal agent, *e.g.* noble metal NPs (20–30 %) [53,55,56] and ICG encapsulated NPs [72,73].

3.2.4. Photoacoustic contrast efficacy of NPs

IR-780 is one of the few NIR absorbing organic dyes that can be utilised in fluorescence, PA, and PTT applications. Therefore, these NPs were established to include IR-780 for both photothermal therapeutic and PA contrast-enhancing function. The photoacoustic contrast-enhancement efficacy of IR-780 encapsulated NPs was determined over a concentration gradient between 9 – 37 μM revealing effective contrast-enhancement over the water control at 9 μM (Fig. 2H-I). This data suggests that the *in vivo* detection limit of the NPs is likely within a μM concentration range. Additionally, whilst most dyes present different absorption and PA spectral maxima, the IR-780 loaded PSI-OA NP PA spectrum does not significantly differ from the absorbance spectrum recorded in water (Fig. 1F), which is an analogous observation to previously reported results for similar nanoemulsions incorporating IR-780 [74].

3.3. Targeting with FA ligand in NPs

These NPs were decorated with FA ligand to target FRα receptors that are highly expressed in various cancer cell types including breast, brain and ovarian cancer. Hence, preliminary screening was performed by evaluating the targeting abilities of our NPs by comparing its uptake (with and without FA ligand) via quantification of fluorescence intensities using Sapphire imaging in various cancer cells lines in comparison to non-malignant cell line (MDA-MB-231, B16F10, MCF-7, Skov-3, U87-MG, HCT-116 and SVEC cells) that are available in our group. All cell lines including non-malignant SVEC cells exhibited increased fluorescence intensities with and without addition of FA targeting ligand in comparison to controls (cells only). The enhanced fluorescence intensity in SVEC cells and the lack of difference in intensity upon FA conjugation suggested that NPs were taken up in SVEC cells via passive uptake due to the limited expression of FRα in non-malignant SVEC cells in comparison to malignant cells [66]. However, U87-MG cells demonstrated the most significant uptake of NPs with FA in comparison to without FA targeting ligand (Fig. 3A). Similarly, a panel of cancer cell lines (MDA-MB-231, B16F10, MCF-7, Skov-3, U87-MG) were incubated with different concentrations of Curcumin loaded PSI-OA NPs with and without FA ligand to evaluate the cytotoxicity of NPs using PrestoBlue assay. In all cancer cell lines, cell viability decreased as concentration of Curcumin increased and the addition of FA ligand resulted in an enhanced cytotoxic killing of all cancer cell lines especially in U87MG cells. The demonstrated augmented uptake and cytotoxicity of targeted NPs is due to the presence of more FRα in cancer cells in comparison to non-malignant cells [66]. At a concentration of 11.2 μg/mL of Curcumin, U87-MG cell viability was 85.3% and the incorporation of FA ligand effected in a significant reduction in cell viability to 35.3% (Fig. 3C). Hence, U87MG cell line was chosen for further analysis based on the heightened uptake and selective killing of targeted NPs in comparison to other cancer cell lines (Fig. 3A, B). Curcumin exhibits intrinsic fluorescence properties when excited at 488 nm wavelength. Fluorescence microscopy images (Fig. 3C) displayed strong innate green fluorescence due to Curcumin in the NPs demonstrating targeting ability of FA decorated dual loaded NPs in U87-MG cells after 1 h incubation in comparison to untreated cells (control).

3.4. Biocompatibility and selectivity of NPs

Non-malignant CHO cells were treated with various concentrations of free Curcumin and Curcumin loaded NPs. At 18.3 μg/mL curcumin, cell viability was at 70.2% with free curcumin and significantly higher at 80% with the PSI-OA loaded Curcumin suggesting reduced toxicity of NPs in non-malignant CHO cells (Fig. 4A). FA conjugated dual loaded NPs were substantially more toxic in U87MG than CHO cells whereby, at 18.3 μg/mL Curcumin and 18.8 μg/mL IR-780, cell viability of CHO cells was 84.9% *versus* U87MG cells at 30.9% (Fig. 4B). Clearly, results obtained here displayed selectivity and cytotoxicity of targeted NPs in U87MG cells due to the over-expression of FRα in cancer cells as opposed to non-malignant CHO cells [75–77]. Also, IR-780 is highly lipophilic and can exert toxicity even in non-malignant cells [78]. Hence, the incorporation of IR-780 in PSI-OA NPs reduces its toxicity in non-malignant cells and potentially minimise associated adverse effects in healthy cells. Notably, NPs exhibited good biocompatibility and that the inclusion of FA targeting ligand effectively and selectively kills cancer cells whilst sparing non-malignant cells.

Haemolysis is defined as the rupture of red blood cells (RBCs) resulting in the release of its contents and subsequently leading to renal malfunction. Hence, haemolytic testing of NPs that are intravenously administered is of utmost importance [79]. Haemocompatibility of FA-PEG conjugated dual loaded NPs was assessed in various concentrations of Curcumin and IR-780 (Fig. 4C). Biomaterials are categorised according to the level of haemolysis: non-haemolytic (0–2% haemolysis), slightly haemolytic (2–5% haemolysis), and haemolytic (>5% haemolysis) [80]. All concentrations of NPs displayed an extremely low level of haemolysis (< 1.5%) including the highest concentration of NPs (Fig. 4 Ci). Triton-X was utilised as the haemolytic agent. No significant haemolysis was induced by the NPs in comparison to Triton-X treated RBCs as illustrated in Fig. 4Cii. Overall, these NPs demonstrated good biocompatibility and are non-haemolytic.

3.5. Cytotoxicity of dual loaded PSI-OA NPs and photothermal ablation in U87-MG cells

Photothermal temperature elevation and cytotoxicity of dual loaded PSI-OA NPs with and without FA targeting ligand were evaluated in U87 MG cells. Cell viability was assessed before and after laser exposure at 2 W/cm^2 for 5 min. At 18.3 and 18.8 μg/mL (Curcumin & IR-780 respectively), cell viability prior to laser irradiation was reduced to 25.9% in FA targeted group and 44.6% in non-targeted group (Fig. 5Aii). Evidently, results obtained displayed a significant killing of U87MG cells with the inclusion of FA ligand due to the heightened uptake of targeted NPs in cancer cells in comparison to non-targeted treatment [66]. Whilst Curcumin has been established as a potent anti-cancer agent, clinical application of Curcumin is hindered by several limitations including low aqueous solubility and rapid metabolism which impedes its full therapeutic potential [9]. Hence, free Curcumin was not included in this cytotoxicity assay. *In vitro* results obtained demonstrated the successful utilisation of PSI-OA as a delivery vehicle to load Curcumin in the treatment of U87MG cells upon addition to the cell culture media. Consequently, as Curcumin has poor water solubility, Curcumin loaded in PSI-OA NPs exhibited high water dispersibility which provided Curcumin with enhanced bioavailability resulting in potent cytotoxicity of NPs in U87MG cells. Additionally, introduction of laser exposure at 2 W/cm^2 for 5 min resulted in a temperature elevation to an average of 57.8 °C and 39.6 °C in targeted and non-targeted groups respectively (Fig. 5Ai). Hence, the addition of FA targeting significantly increased the temperature by an average of 18.2 °C proposing a better uptake of targeted NPs in U87MG cells which resulted in an enhanced temperature increment upon laser irradiation. Untreated (control) cells that were exposed to laser irradiation displayed no significant increase in temperature. Cytotoxicity was ascertained after laser treatment and cell death was at approximately 100% and 85.4% in targeted and

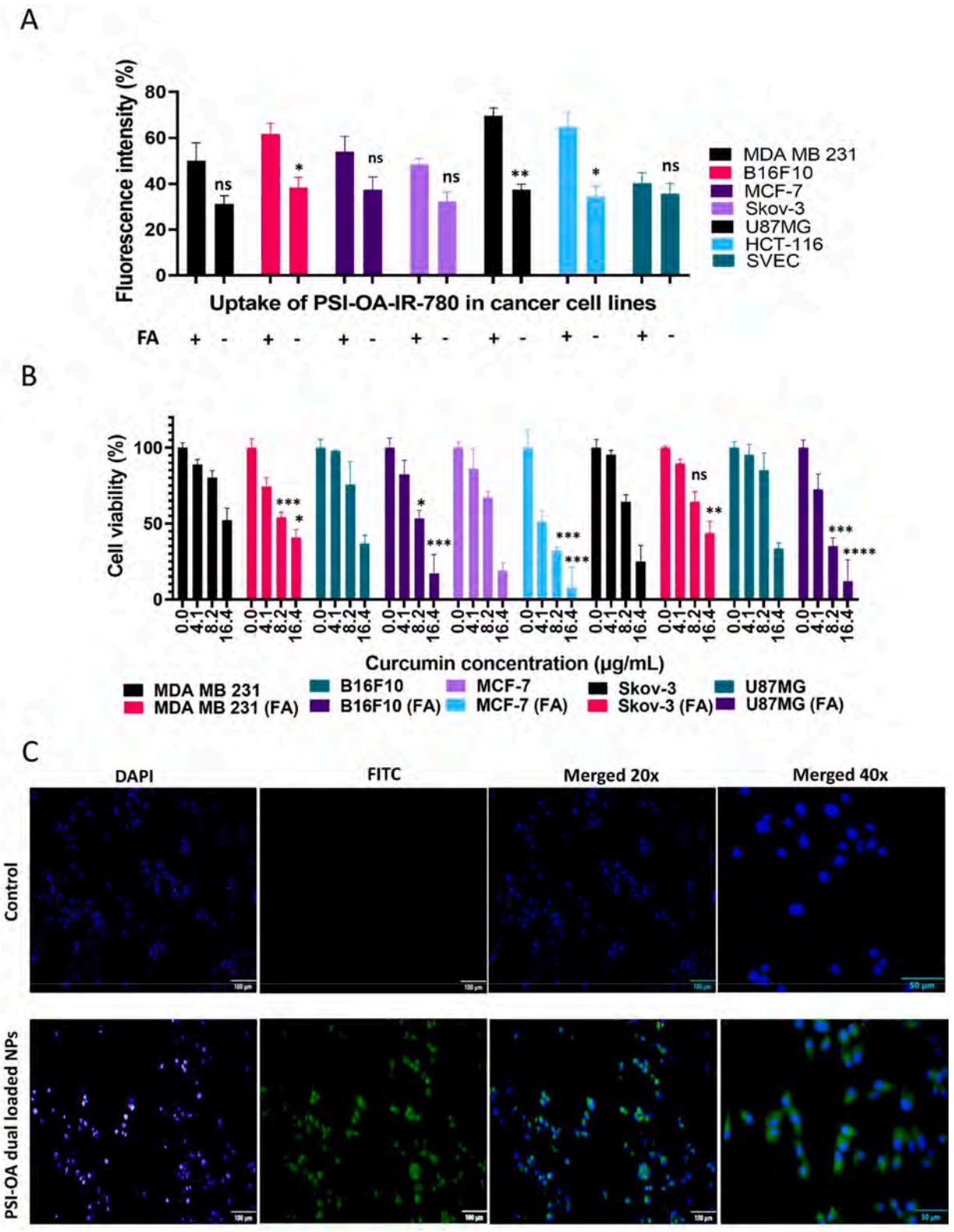

Fig. 3. Targeting with and without FA ligand in NPs. A) A panel of cell lines were incubated with PSI-OA loaded with IR-780 for 4 h. Uptake of NPs was represented by the fluorescence intensity measured using Sapphire system. * Compared with targeted NPs. * $p < 0.05$, ** $p < 0.01$, B) A panel of cancer cell lines were treated with PSI-OA loaded with Curcumin with and without FA ligand at varying Curcumin concentrations for 24 h. * Compared with non-targeted NPs at respective concentrations. * $p < 0.05$, ** $p < 0.01$, *** $p < 0.001$, **** $p < 0.0001$ C) Fluorescence images of U87MG cells only (control) and labelled with 18.3 μg/mL (Curcumin) of complete FA conjugated PSI-OA dual loaded NPs (18.3 μg/mL curcumin and 18.8 μg/mL IR780) for 1 h. The nuclei were stained with DAPI (blue) and Curcumin (green FITC): 20x and 40x magnification.

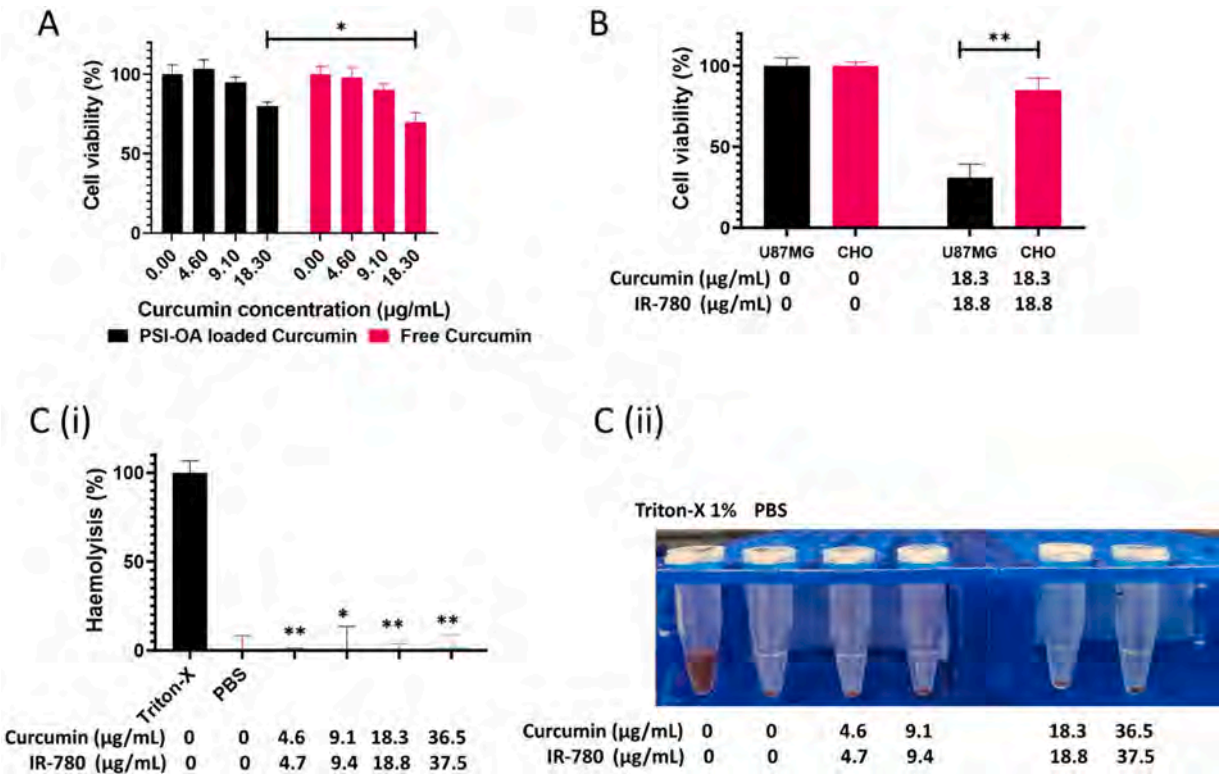

Fig. 4. Biocompatibility and selectivity of NPs. (A) CHO cells were treated with PSI-OA loaded with Curcumin and free Curcumin for 12 h. * Compared with free Curcumin. * $p < 0.05$ (B) U87MG and CHO cells were treated with FA conjugated PSI-OA NPs loaded with Curcumin and IR-780 dye for 12 h. * Compared with CHO cells. ** $p < 0.01$ (C) Haemolysis assay of red blood cells incubated with increasing concentrations of FA-PEG conjugated PSI-OA NPs loaded with Curcumin and IR-780 dye after 1 h incubation. * Compared to Triton-X treatment. * $p < 0.05$, ** $p < 0.01$ (ii) Representative images.

non-targeted groups respectively (Fig. 5Aii). Also, Curcumin has been shown to inhibit the expression of heat shock protein 90 which functions to allow cancer cells to develop thermal tolerance, hence reducing sensitivity of cells to photothermal laser exposure [81]. Consequently, Curcumin can effectively reduce thermal tolerance of cancer cells making them more susceptible to laser irradiation. Notably, data obtained revealed that FA targeting clearly enhanced both the uptake and cytotoxicity of NPs whilst laser exposure ensued a further significant synergistic obliteration of U87MG cells *in vitro*.

Additionally, U87MG cells treated with NPs only and the incorporation of laser irradiation were assessed to quantify the apoptotic and necrotic cell populations via the utilisation of Annexin V-FITC Apoptosis Detection Kit. The untreated cells (control) displayed a viable cell population of 99.5% whilst the apoptotic and necrotic cells were negligible (Figs. 5B and S3). After NPs treatment, viable cell population significantly decreased to < than 5% with predominant cell population in early apoptotic at 60.3 % and late apoptotic stage at 35.5% suggesting the potent cytotoxicity of these dual loaded NPs. After laser irradiation, early apoptotic cell population decreased to 26.1% and the late apoptotic/necrotic cell population increased to 64.9%. These results indicated that the incorporation of laser irradiation resulted in the shift of cell populations to late-stage apoptosis which resulted in a further synergistic killing of U87MG cells which corroborates with the results acquired from the previous cell viability assay (Fig. 5A)

3.6. *In vivo biosafety assessment*

PSI-OA NPs loaded with Curcumin and IR-780 were evaluated for its biosafety in C57/BL6J mice. These mice were intravenously infused with three doses of NPs at 2 concentrations of 3.7/3.8 and 7.3/7.5 mg/kg of Curcumin and IR-780 respectively. Control group was referred to as saline treated mice. Body weights of mice in 3.7/3.8 mg/kg (Curcumin & IR-780 respectively) revealed no significant difference in comparison to control groups (Fig. 6A). At double the concentration, body weights of mice started to decrease after the second dose of treatment but increased progressively till the end of the experiments whereby weights recorded displayed no substantial difference when compared to control mice. Mice were sacrificed 12 days after initiation of treatment with major organs and blood serum collected for further biosafety analysis. The organ weights of the liver, heart, spleen, lungs and kidneys were measured and Fig. 6B represents the relative organ weight in regard to the total body weight of mice. Only the liver displayed an increased in weight with increasing concentration of NPs in comparison to the control group albeit not statistically significant. Based on the size of the NPs (~220 nm), they are most likely cleared via the hepatobiliary or mononuclear phagocyte system (MPS) hence some accumulations of NPs are expected in the liver. The rest of the organs from treatment groups exhibited no substantial difference in relative organ weight. Consequently, biochemical analysis of kidney function markers including creatinine, urea and uric acid and liver function markers such as bilirubin, ALT, glucose and albumin were measured accordingly (Fig. 6Ci-vii). Glucose levels increased in both NP treatment groups but was still within healthy acceptable range (Fig. 6 Ci). In comparison to the control group, TBIL and DBIL levels decreased in the 3.7/3.8 mg/kg (Curcumin and IR-780 respectively) and 7.3/7.5 mg/kg groups (Curcumin and IR-780 respectively). Nonetheless, bilirubin levels acquired are still within healthy acceptable range (Fig. 6Cii). Albumin and creatinine levels did not differ much between treatment groups (Fig. 6Ciii and v). Whilst a slight decrease in the levels of ALT, urea and uric acid was observed in treatment groups in comparison to control group, levels are still within a healthy acceptable range (6Civ, vi and vii). Tissues of main organs such as the liver, heart, spleen, lungs and kidneys were stained with H & E for imaging. Fig. 6D of tissues illustrate no discernible impairment or inflammation even at the highest

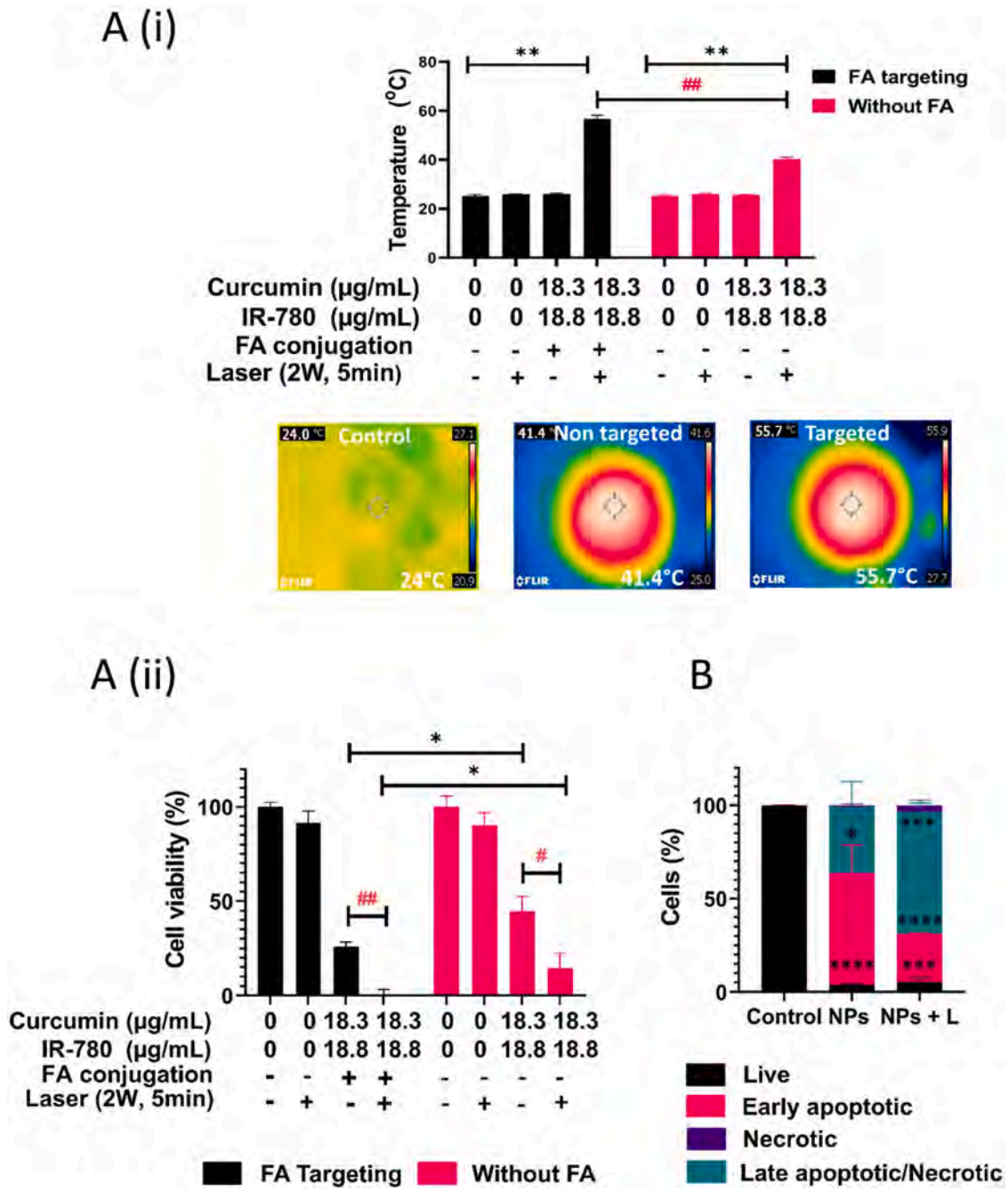

Fig. 5. Cytotoxicity of cells incubated with NPs with and without FA targeting (A) U87MG cells incubated with dual loaded PSI-OA NPs with and without FA targeting and exposed to laser irradiation at 2 W/cm^2, 5 min. (i) Photothermal temperature elevation and corresponding representative NIR thermographic images of the wells at the 60th second. * Compared with control (No NPs and no laser). ** $p < 0.01$, # Compared with the addition of FA targeting. ## $p < 0.01$. (ii) Photothermal cytotoxicity in U87MG cells with and without laser. * Compared to respective groups with and without FA targeting. * $p < 0.05$. # Compared to the addition of laser exposure. # $p < 0.05$, ## $p < 0.01$. (B) Flow cytometry analysis of U87MG cells treated with 18.3 and 18.8 μg/mL of Curcumin and IR-780 respectively to determine stages of apoptosis, laser (L) irradiation at 2 W/cm^2, 5 min. * Compared to the respective stages of apoptosis cell population of the control group: * $p < 0.05$, *** $p < 0.001$, **** $p < 0.0001$.

concentration of NPs at (7.3/7.5 mg/kg of Curcumin and IR-780 respectively). Overall, repeated doses of highly concentrated dual loaded NPs did not result in significant adverse effect and toxicity to the major organs of mice.

3.7. *In vivo* therapeutic and photothermal efficacy

In total, there were 4 treatment groups which involved the intravenous administration of 1) saline (control), 2) NPs only, 3) FA conjugated NPs only and 4) FA conjugated NPs plus laser treatment. The efficacy of treatment groups was assessed in comparison to saline treated control group. Treatment was initiated when the tumour volume reached >100 mm^3. Mice were injected with NPs at 0.9 mg/kg of Curcumin and IR-780 each at 3 doses at Day 0, 7 and 14 via the tail vein. It should be noted that the dose administered here is much lesser in comparison to the dose infused in the biosafety assessment studies described above. For the laser group, mice were exposed to laser irradiation at 1.5 W/cm^2 for 5 min, 24 h after the injection of NPs. A thermal camera was utilised to capture the

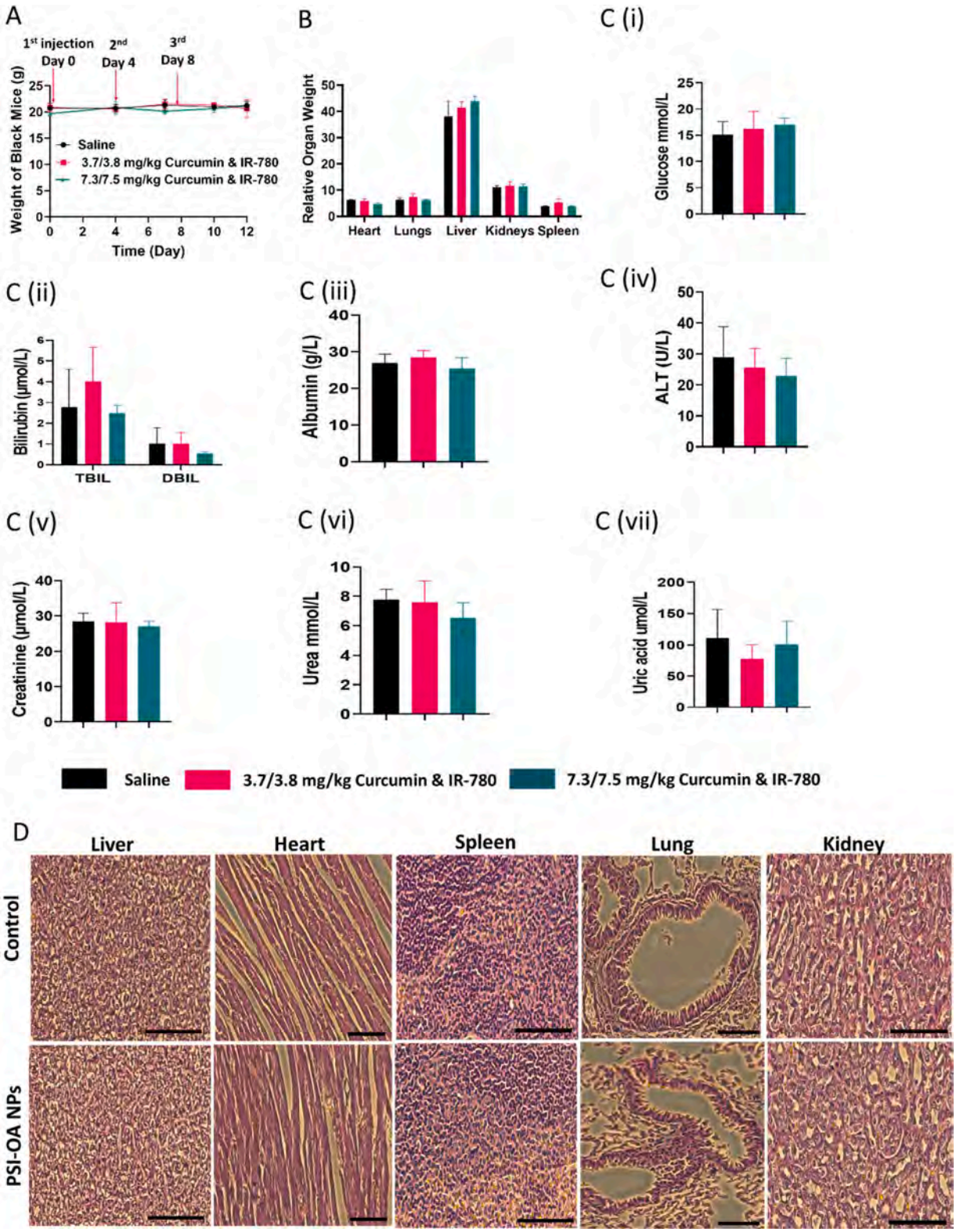

Fig. 6. Biosafety studies of NPs in female C57BL/6 J mice. Mice were injected intravenously with saline (control group), PSI-OA dual loaded with Curcumin (3.7 mg/kg and 7.3 mg/kg respectively) & IR-780 (3.8 mg/kg and 7.5 mg/kg respectively) at Day 0, 4 and 8 to determine the *in vivo* biocompatibility of the nanoparticles. (A) Average body weight of mice monitored twice a week across the experimental period. (B) Organs including heart, lungs, liver, kidneys and spleen were collected and weighted at Day 12. Relative organ weights (organ-weight-to-body-weight ratios) were determined as mg organ weight/g terminal body weight of mice. (C) Blood samples were collected at Day 12 via cardiac puncture. Serum samples from whole blood collected were tested for (i) Glucose, (ii) Bilirubin, (iii) Albumin, (iv) Alanine transaminase (ALT), (v) Creatinine, (vi) Urea and (vii) Uric acid. D) Histological images of tissues stained with H & E indicating the status of major organs after animals were sacrificed at Day 12 post i.v. injection. Scale bar: 100 μm.

temperature changes. The tumour volume and weights of all mice were recorded every alternate day throughout the length of the experiment. Fig. 7A displayed no significant distinction in body weights of treatment groups in comparison to control group suggesting that mice were not adversely affected by NPs or laser exposure. Tumours in control group continued to proliferate and grow over time. Contrastingly, all treatment groups exhibited a substantial reduction in tumour growth and were significantly smaller to control group (Fig. 7B–D). Whilst FA targeting did not result in a significant improvement in tumour reduction in comparison to non-targeted group, the inclusion of laser irradiation effected in a temperature rise to an average of 48 °C which caused an irreversible damage to the tumour cells. Consequently, incorporation of laser treatment imposed a significant synergistic cytotoxicity of tumours based on the terminal tumour weights (Fig. 7B–D). Interestingly, Yuan et al. reported that intravenously infused micelle loaded IR-780 NPs (7 mg/kg of IR-780) significantly eliminated CT 26 tumours *in vivo* after laser exposure at 1 W/cm^2 for 10 min which resulted in a maximal temperature acquisition of 52.5 °C [65]. Another study by Wang and colleagues displayed that intravenous injection of self-assembled IR-780 NPs (20 mg/kg of IR-780) functionalised with transferrin resulted in significant CT 26 tumour reduction *in vivo* post laser irradiation at 1 W/cm^2 for 5 min which effected in a temperature rise to 49.5 °C [82]. Concentrations of IR-780 injected in both studies are 7.8 and 22.2 times correspondingly the concentration (0.9 mg/kg of IR-780) we used in our *in vivo* studies. Consequently, our dual loaded NPs demonstrated significant photothermal tumour ablation with a maximal temperature elevation to 48 °C despite a lower concentration of IR-780 partly due to the incorporation of Curcumin and the inclusion of FA targeting ligand which further imparted inherent anti-cancer abilities and enhanced accumulation in tumours respectively. Notably, the adjacent regions of the tumour did not display any discernible signs of burns visually and mice appeared healthy and happy throughout the experimental period. Saline treated mice exposed to laser irradiation demonstrated a temperature elevation to a maximal of 35 °C which was insufficient to cause any irrevocable damage (Fig. 7D). The NPs plus laser treatment group demonstrated a temperature acquisition of an average of 13 °C higher than control group hence signifying efficient migration of NPs into the tumours and proficient photothermal capability of NPs resulting in the ablation of tumour *in vivo* (Fig. 7C–D). Fig. 7E illustrates tumours that are stained with TUNEL of control, treatment with NPs only and NPs plus laser exposure. Control group displayed a healthy and confluent tumour cell morphology. Following NP treatment, cancer cells looked contracted, with a condensed chromatin and demonstrated some distinct brown stains. Hence, NP treatment induced stress and exhibited hallmarks of early and late apoptosis which corroborates data from the *in vitro* apoptotic analysis (Fig. 5C). Tumours from the NPs plus laser treatment group displayed apparent and more significant brown stains indicating DNA and nuclear disintegration which arises in late-stage apoptosis. Overall, these *in vivo* results established that FA conjugated PSI-OA dual loaded NPs with the accompaniment of laser exposure, provides a powerful and effective approach in the treatment of U87MG tumours. As *in vivo* studies were performed in a subcutaneous U87MG model, further evaluation of treatment efficacy needs to be assessed in an orthotopic glioma model.

3.8. *In vivo targeting and PA and fluorescence imaging efficacy*

Subsequently, we also assessed the efficacy of our dual loaded NPs as a PA imaging contrast agent and evaluated the targeting ability of FA ligand using MSOT and fluorescence imaging *in vivo*. IVIS imaging based on IR-780 dye were performed 30 min, 24 h, 48 h and 6 days post injection of NPs. At 30 min timepoint, both targeted and non-targeted NPs accumulated in the liver. 24 h later, fluorescence intensity in the tumour region increased in both targeted and non-targeted groups and some accumulation was observed in the liver (Fig. 8A). Nevertheless, a significant difference in fluorescence intensity was observed between targeted and non-targeted groups, highlighting the heightened accumulation of targeted FA NPs in the tumours (Fig. 8C). A major challenge in the development and application of nanotheranostic is the localisation of NPs in the hepatic tissues resulting in low accumulation in targeted disease site leading to inefficient therapeutic outcome [83]. Hence, strategies to adjourn, reduce or totally prevent the clearance of NPs via the MPS could lead to an enhanced treatment efficacy [83]. Here, our NPs displayed a significant localisation in the tumours at 24 h, 48 h and Day 6 post injection. Interestingly, NPs injected in mice with no tumour displayed fluorescence intensity ubiquitously suggesting the enhanced selectivity and accumulation of these NPs in tumours as displayed in Fig. 8A. At 48 h post administration of NPs, fluorescence intensity decreased in tumours and liver of both groups of mice with targeted group demonstrating a higher intensity in comparison to non-targeted group. Subsequently, at Day 6, fluorescence intensity in tumours and liver reduced further in both groups of mice, however, tumours from targeted group displayed a statistically significant difference in comparison to non-targeted group suggesting an enhanced retention of NPs in tumours at Day 6.

MSOT imaging performed at Day 0, 24 h and 48 h post-injection provided strong evidence of NP accumulation within the tumours (Fig. S4A). Both targeted and non-targeted groups demonstrated a significant increase in the 790 nm mean pixel intensity (MPI) measured at the centre of the tumour 24 h post-administration (Fig. S4B). Hence, these results depict NP accumulation in tumours through both active receptor facilitated and passive pathways. The former is accomplished by the presence of FA ligand which binds firmly to FRα that are highly expressed in some cancer cells [38]. The latter is achieved via the enhanced permeability and retention effect which is also assisted by the PEGylation of the NPs which allows non-targeted NPs to escape through the leaky blood vessels and localise within the tumour [37]. Furthermore, PSI-OA NP accumulation within tumours was also uncovered by spectrally unmixing endogenous and exogenous components to specifically identify PSI-OA NPs within the cancerous tissue. Spectral unmixing is particularly important for the identification of relevant endogenous and exogenous components to accurately resolve anatomical features and areas of exogenous agent accumulation [84]. Unmixed MSOT images (Fig. 8B) present PSI-OA, HbO_2 and Hb at equivalent thresholding values to demonstrate the relative detection sensitivities of each component. The unmixed PSI-OA NP signal appears to present a lower detection sensitivity relative to the high endogenous background signal, resulting in minimal PSI-OA NP signal visualised within tumour volumes at the image thresholding limit. The low detection sensitivity of the IR-780 loaded PSI-OA NP relative to the endogenous background may be a result of the optoacoustic signal intensity per IR-780 molecule decreasing upon loading into nano emulsions, as has been previously reported for IR-780 [74]. Nevertheless, quantitative analysis of the unmixed MSOT images reveals spectrally unmixed PSI-OA NP signal within the cancerous tissue whereby the FA targeted group presented significantly higher signal assigned to the PSI-OA NP channel within the tumours compared to the non-targeted group. Fig. 8D presents the sum of the pixel values assigned to the PSI-OA NP channel within the tumour volume normalised to the baseline PSI-OA NP signal established at day 0, revealing a 4-fold increase in PSI-OA NP signal for the targeted group compared to non-targeted at 24 h. Thus, MSOT imaging provided strong evidence that incorporation of FA targeting ligands enhanced the tumour accumulation of our PSI-OA NPs.

Both FI and MSOT imaging data infer maximum NP tumour accumulation is achieved in less than 48 h post-injection of NPs (Fig. 8C& D). Hence, photothermal therapy was induced at 24 h post-injection of NPs to achieve maximum photothermal efficacy (Fig. 7). Even though there was a decrease in signal associated with PSI-OA NP in both groups at 48 h post injection of NPs, the FI and MSOT signal associated with the PSI-OA NP was still statistically significant in comparison to signal attained at Day 0, indicating retention of NPs (Fig. S4B). Overall, both imaging modalities revealed an increased signal in comparison to pre-injection

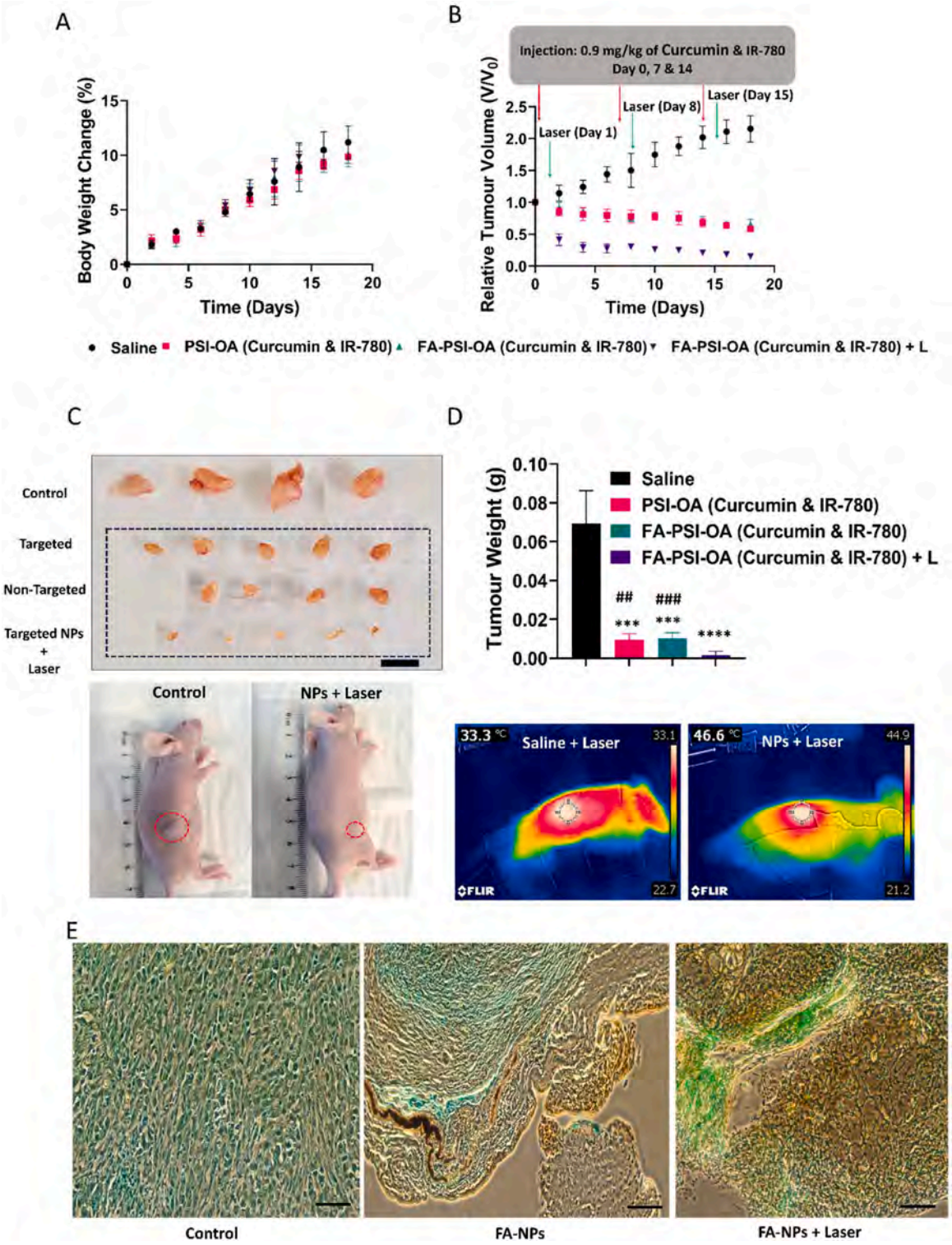

Fig. 7. *In vivo* therapeutic effects of PSI-OA dual loaded with Curcumin & IR-780 with and without FA targeting and laser irradiation at (1.5 W/cm^2, 5 min) in U-87 MG tumour-bearing BALB/C mice. Mice were injected intravenously with Saline (control group), dual loaded PSI-OA NPs (0.9 mg/kg of Curcumin and IR-780 each), FA conjugated dual loaded PSI-OA (0.9 mg/kg of Curcumin and IR-780 each), at three time-points (Day 0, 7 and 14). (A) Average body weight of mice monitored twice a week during the treatment. Mice body weight analysed with repeated measures one-way ANOVA with Tukey's multiple comparisons demonstrated no significant changes in all treatment groups across the experimental period. (B) Changes in tumour volume during the experiment period. Relative tumour volume was defined as tumour volume (V_0) measured normalised to tumour volume at Day 0 before administration of treatment (V_0). Treatment and laser exposure days depicted via red and green arrows respectively. (C) Images of tumours harvested at Day 18 post administration of NPs. Scale bar: 10 mm. (D) Terminal tumour weight and representative thermal images of mice after laser exposure. * Compared to saline: *** $p < 0.001$, **** $p < 0.0001$. # Compared to FA conjugated NPs + Laser: ## $p < 0.01$, ### $p < 0.001$ (E) Histological images of tumour tissues stained with TUNEL. Scale bar: 100 μm.

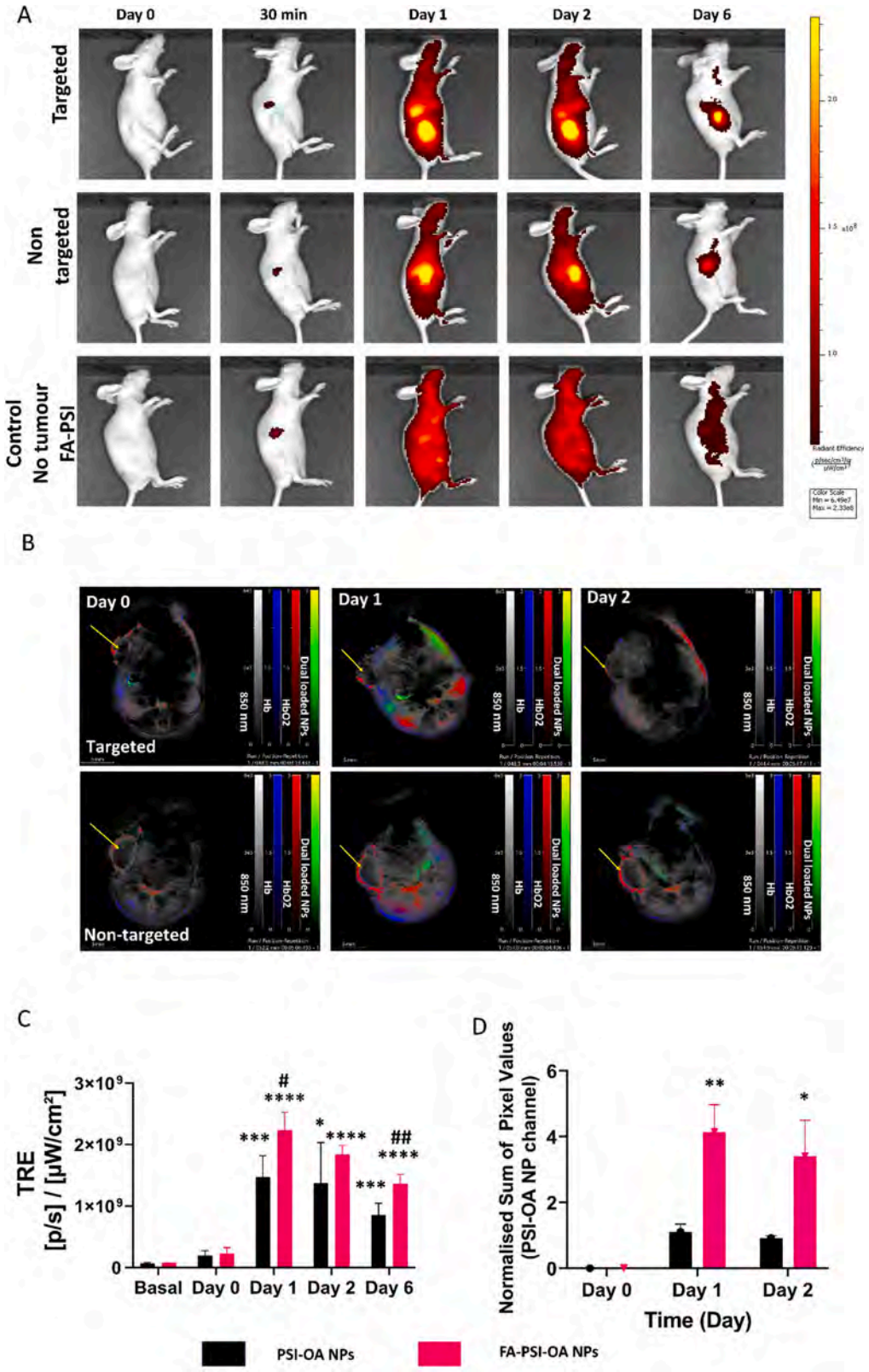

Fig. 8. *In vivo* tumour targeting (PAI and fluorescence imaging) of dual loaded PSI-OA NPs and FA conjugated dual loaded PSI-OA in U-87 MG tumour-bearing BALB/C mice. Mice were injected intravenously. (A) Representative images of mice using fluorescence imaging. Mouse tumours were imaged before (Day 0), immediately post-injection, 1-, 2- and 6- days post injection of NPs. (B) Representative images of spectrally unmixed MSOT images at the centre of the tumour volume acquired at Day 0, 1 and 2. Hb: Haemoglobin, HbO2: Oxyhaemoglobin. (C) Total radiant efficiency of mice tumours over time. * Compared with pre injection at Day 0. * $p < 0.05$, *** $p < 0.001$, **** $p < 0.0001$. # Compared with non-targeted group. # $p < 0.05$, # $p < 0.01$. (D) Quantitative analysis of unmixed MSOT images presenting the normalised sum of the pixel value assigned to the dual loaded PSI-OA NPs channel by the multispectral unmixing algorithm. Data acquired from a single image frame set at the centre of the tumour volume and normalised to the baseline signal at day 0. * Compared with non-targeted group. * $p < 0.05$, ** $p < 0.01$. $n = 3$.

Day 0 and importantly demonstrated a statistically significant difference between targeted and non-targeted groups.

Our PA and FI results demonstrated the successful utilisation of both imaging modalities with our NPs and underscores the importance of the utilisation of multiple imaging tool whereby drawbacks associated with individual techniques can be overcome [32]. This approach encompasses the development of multifunctional NPs whereby complementary roles of each technique can be fully exploited.

Ultimately, Curcumin and IR-780 have both been individually established for promising therapeutic strategies for the treatment of cancerous tissue, whereby the former presents intrinsic anti-cancer properties and the latter serves as a potent PTT agent [33,85]. However, their individual clinical application is impeded by several drawbacks including low aqueous solubility and rapid metabolism which hampers their therapeutic efficacy [11,65]. Therefore, our approach to simultaneously encapsulate Curcumin and IR-780 into FA functionalised PSI-OA NPs not only tackles these limitations but results in heightened selective targeting, accumulation and retention in tumours.

4. Conclusion

We have successfully developed a novel oleylamine-modified PSI NP which performs as a carrier for Curcumin and IR-780 dye and is aimed to address limitations associated with the clinical application of these agents by improving their bioavailability, circulation half-life, serum stability, and therapeutic efficacy. The NPs presented herein displayed high Curcumin and IR-780 encapsulation efficiency and a drug release profile that is in agreement with the particle dissolution profile, whereby NPs remained stable and started to release Curcumin and IR-780 after 8.5 h with maximal release after 36 h at pH 7.4. Interstingly, burst release of drugs was not observed, which is a major advantage of our nanosystems. Targeting folate receptors on cancer cells and the incorporation of laser irradiation significantly improved selectivity and therapeutic efficacy of NPs both *in vitro* and *in vivo*. Consequently, our targeted dual loaded NPs could mostly eradicate U87MG tumours after three weekly low dose intravenous infusion revealing its outstanding anti-cancer accomplishment. Importantly, encapsulation of Curcumin and IR-780 into PSI-OA NPs improved the bioavailability, and tumour retention of Curcumin and IR-780. Biosafety and biochemical assessment of NPs presented no apparent toxicity *in vitro* and *in vivo*. Our future work involve the assessment of the pharmacokinetic of our NPs *in vivo* and the therapeutic application in an orthotopic glioma model. Overall, our dual loaded PSI-OA NPs demonstrated outstanding potential as a powerful and safe theranostic strategy for synergistic folate receptor targeted chemo-photothermal treatment and bimodal MSOT and fluorescence imaging.

Data availability statement

Data will be made available on request from the authors.

CRediT authorship contribution statement

Shehzahdi S. Moonshi: Writing – original draft, Writing – original draft, Visualization, Methodology, Investigation, Formal analysis. **Karla X. Vazquez-Prada:** Investigation. **Hossein Adelnia:** Methodology, Investigation. **Nicholas J. Westra van Holthe:** Methodology, Investigation. **Yuao Wu:** Investigation. **Joyce Tang:** Investigation. **Andrew C. Bulmer:** Methodology, Investigation. **Hang Thu Ta:** Writing – review & editing, Supervision, Resources, Project administration, Methodology, Funding acquisition, Conceptualization.

Declaration of competing interest

The authors declare the following financial interests/personal relationships which may be considered as potential competing interests:

Hang Thu Ta reports financial support was provided by National Health and Medical Research Council. Hang Thu Ta reports financial support was provided by National Heart Foundation of Australia.

Data availability

Data will be made available on request.

Acknowledgement

This work is funded by National Health and Medical Research Council (HTT: APP1182347, APP2002827). SSM is supported by a Griffith University postdoctoral fellowship. KVP and HA are supported by PhD scholarships from the University of Queensland. HTT is supported by a Heart Foundation Future Leader Fellowship (102761). The authors would like to acknowledge the Australian National Fabrication Facility (Queensland Node) access to key items of equipment. The authors acknowledge the facilities and scientific and technical assistance of the National Imaging Facility, a National Collaborative Research Infrastructure Strategy (NCRIS) capability, at the Centre for Advanced Imaging and School of Chemistry and Molecular Biosciences University of Queensland.

Supplementary materials

Supplementary material associated with this article can be found, in the online version, at doi:10.1016/j.apmt.2024.102150.

References

[1] H. Yan, et al., Neoadjuvant nano-photothermal therapy used before operation effectively assists in surgery for breast cancer, Nanoscale 11 (2) (2019) 706–716.
[2] S.S. Moonshi, et al., Placenta-derived mesenchymal stem cells for treatment of diseases: a clinically relevant source, Adv. Ther. 5 (10) (2022) 2200054 (Weinh).
[3] S.S. Moonshi, et al., A comparison of PET imaging agents for the assessment of therapy efficacy in a rodent model of glioma, Am. J. Nucl. Med. Mol. ImAging 3 (5) (2013) 397–407.
[4] R. Bejot, et al., Aminooxy-functionalized DOTA for radiolabeling of oxidized antibodies: evaluation of site-specific 111In-labeled trastuzumab, J. Label. Compd. Radiopharm. 55 (9) (2012) 346–353.
[5] C. Zhang, et al., High F-content perfluoropolyether-based nanoparticles for targeted detection of breast cancer by 19F magnetic resonance and optical imaging, ACS Nano 12 (9) (2018) 9162–9176.
[6] N.S. Srivastava, R.A.K. Srivastava, Curcumin and quercetin synergistically inhibit cancer cell proliferation in multiple cancer cells and modulate Wnt/β-catenin signaling and apoptotic pathways in A375 cells, Phytomedicine 52 (2019) 117–128.
[7] E.C. Filippi-Chiela, et al., Autophagy interplay with apoptosis and cell cycle regulation in the growth inhibiting effect of resveratrol in glioma cells, PLoS One 6 (6) (2011) e20849.
[8] S. Zhao, et al., Curcumin-loaded redox response of self-assembled micelles for enhanced antitumor and anti-inflammation efficacy, Int. J. Nanomed. 12 (2017) 2489–2504.
[9] D.H. Hanna, G.R. Saad, Nanocurcumin: preparation, characterization and cytotoxic effects towards human laryngeal cancer cells, RSC Adv. 10 ((35) (2020) 20724–20737.
[10] A. Giordano, G. Tommonaro, Curcumin and cancer, Nutrients 11 (10) (2019).
[11] A. Shehzad, F. Wahid, Y.S. Lee, Curcumin in cancer chemoprevention: molecular targets, pharmacokinetics, bioavailability, and clinical trials, Arch. Pharm. 343 (9) (2010) 489–499 (Weinheim).
[12] H. Adelnia, et al., Freeze/thawed polyvinyl alcohol hydrogels: present, past and future, Eur. Polym. J. 164 (2022) 110974.
[13] E. Jalalvandi, A. Shavandi, Polysuccinimide and its derivatives: degradable and water soluble polymers (review), Eur. Polym. J. 109 (2018) 43–54.
[14] G. Cavallaro, et al., Synthesis and characterization of polyaspartamide copolymers obtained by ATRP for nucleic acid delivery, Int. J. Pharm. 466 (1) (2014) 246–257.
[15] G. Cavallaro, et al., Galactosylated polyaspartamide copolymers for siRNA targeted delivery to hepatocellular carcinoma cells, Int. J. Pharm. 525 (2) (2017) 397–406.
[16] S. Currie, et al., Mucus-penetrating PEGylated polysuccinimide-based nanocarrier for intravaginal delivery of siRNA battling sexually transmitted infections, Colloids Surf. B Biointerfaces 196 (2020) 111287.
[17] H. Adelnia, et al., Poly(succinimide) nanoparticles as reservoirs for spontaneous and sustained synthesis of poly(aspartic acid) under physiological conditions: potential for vascular calcification therapy and oral drug delivery, J. Mater. Chem. B (2023).

[18] K.Y. Choi, et al., Theranostic nanoplatforms for simultaneous cancer imaging and therapy: current approaches and future perspectives, Nanoscale 4 (2) (2012) 330–342.
[19] J.L.Y. Tang, S.S. Moonshi, H.T. Ta, Nanoceria: an innovative strategy for cancer treatment, Cell Mol. Life Sci. 80 (2) (2023) 46.
[20] Y. Wu, et al., Recent advances in the development of theranostic nanoparticles for cardiovascular diseases, Nanotheranostics 5 (4) (2021) 499.
[21] Y. Wu, et al., Engineering chitosan nano-cocktail containing iron oxide and ceria: a two-in-one approach for treatment of inflammatory diseases and tracking of material delivery, Mater. Sci. Eng. C 131 (2021) 112477.
[22] K.X. Vazquez-Prada, et al., Photothermal nanomaterials for theranostics of atherosclerosis and thrombosis, Appl. Mater. Today 35 (2023) 101967.
[23] M. Zhou, et al., A chelator-free multifunctional [64Cu]CuS nanoparticle platform for simultaneous micro-PET/CT imaging and photothermal ablation therapy, J. Am. Chem. Soc. 132 (43) (2010) 15351–15358.
[24] S.C. Gad, et al., Evaluation of the toxicity of intravenous delivery of auroshell particles (gold-silica nanoshells), Int. J. Toxicol. 31 (6) (2012) 584–594.
[25] D. Gao, et al., Targeting hypoxic tumors with hybrid nanobullets for oxygen-independent synergistic photothermal and thermodynamic therapy, Nanomicro Lett. 13 (1) (2021) 99.
[26] C.S. Jin, et al., Ablation of hypoxic tumors with dose-equivalent photothermal, but not photodynamic, therapy using a nanostructured porphyrin assembly, ACS Nano 7 (3) (2013) 2541–2550.
[27] M. Kim, et al., Numerical study on effective conditions for the induction of apoptotic temperatures for various tumor aspect ratios using a single continuous-wave laser in photothermal therapy using gold nanorods, Cancers 11 (6) (2019) (Basel).
[28] E. Zhang, et al., Mechanistic study of IR-780 dye as a potential tumor targeting and drug delivery agent, Biomaterials 35 (2) (2014) 771–778.
[29] Z. Yang, et al., Long-circulating near-infrared fluorescence core-cross-linked polymeric micelles: synthesis, characterization, and dual nuclear/optical imaging, Biomacromolecules 8 (11) (2007) 3422–3428.
[30] I. Steinberg, et al., Photoacoustic clinical imaging, Photoacoustics 14 (2019) 77–98.
[31] J.V. Frangioni, *In vivo* near-infrared fluorescence imaging, Curr. Opin. Chem. Biol. 7 (5) (2003) 626–634.
[32] S.S. Moonshi, Y. Wu, H.T. Ta, Visualizing stem cells *in vivo* using magnetic resonance imaging, WIREs Nanomed. Nanobiotechnol. (2021) e1760, n/a(n/a).
[33] C. Yue, et al., IR-780 dye loaded tumor targeting theranostic nanoparticles for NIR imaging and photothermal therapy, Biomaterials 34 (28) (2013) 6853–6861.
[34] H. Fasehee, et al., Delivery of disulfiram into breast cancer cells using folate-receptor-targeted PLGA-PEG nanoparticles: *in vitro* and *in vivo* investigations, J. Nanobiotechnol. 14 (1) (2016) 32.
[35] C.K. Elechalawar, et al., Dual targeting of folate receptor-expressing glioma tumor-associated macrophages and epithelial cells in the brain using a carbon nanosphere–cationic folate nanoconjugate, Nanoscale Adv. 1 (9) (2019) 3555–3567.
[36] U. Agrawal, et al., Tailored polymer–lipid hybrid nanoparticles for the delivery of drug conjugate: dual strategy for brain targeting, Colloids Surf. B Biointerfaces 126 (2015) 414–425.
[37] J.S. Suk, et al., PEGylation as a strategy for improving nanoparticle-based drug and gene delivery, Adv. Drug Deliv. Rev. 99 (2016) 28–51 (Pt A).
[38] L.S.F. Boogerd, et al., Concordance of folate receptor-α expression between biopsy, primary tumor and metastasis in breast cancer and lung cancer patients, Oncotarget 7 (14) (2016). Vol.
[39] S. Bhattacharjee, Understanding the burst release phenomenon: toward designing effective nanoparticulate drug-delivery systems, Ther. Deliv. 12 (1) (2020) 21–36.
[40] H.T. Ta, et al., A chitosan hydrogel delivery system for osteosarcoma gene therapy with pigment epithelium-derived factor combined with chemotherapy, Biomaterials 30 (27) (2009) 4815–4823.
[41] X. Chen, et al., Polymeric nanomaterial strategies to encapsulate and deliver biological drugs: points to consider between methods, Biomater. Sci. 11 (6) (2023) 1923–1947.
[42] X. Chen, et al., Preparation of protein-loaded nanoparticles based on poly (succinimide)-oleylamine for sustained protein release: a two-step nanoprecipitation method, Nanotechnology 35 (5) (2023) 055101.
[43] X. Huang, C.S. Brazel, On the importance and mechanisms of burst release in matrix-controlled drug delivery systems, J. Control. Release 73 (2) (2001) 121–136.
[44] J.A. Setterstrom, et al., Development of encapsulated antibiotics for topical administration to wounds, in: Proceedings of the Transactions of the Annual Meeting of the Society for Biomaterials in Conjunction with the International Biomaterials Symposium, 1984.
[45] X. Bai, et al., Sustained drug release from smart nanoparticles in cancer therapy: a comprehensive review, Micromachines 13 (2022), https://doi.org/10.3390/mi13101623 (Basel).
[46] H. Adelnia, et al., A bioactive disintegrable polymer nanoparticle for synergistic vascular anticalcification, ACS Nano (2023).
[47] S. Bhattacharjee, DLS and zeta potential – what they are and what they are not? J. Control. Release 235 (2016) 337–351.
[48] S.S. Moonshi, et al., Spiky silver–iron oxide nanohybrid for effective dual-imaging and synergistic thermo-chemotherapy, ACS Appl. Mater. Interfaces (2023).
[49] S. Zhang, C. Wang, Precise analysis of nanoparticle size distribution in TEM image, Methods Protoc. 6 (2023), https://doi.org/10.3390/mps6040063.
[50] R.S. Pandit, et al., Curcumin nanoparticles: physico-chemical fabrication and its *in vitro* efficacy against human pathogens, 3 Biotech. 5 (6) (2015) 991–997.
[51] S. Solghi, et al., The encapsulation of curcumin by whey protein: assessment of the stability and bioactivity, J. Food Process. Eng. 43 (6) (2020) e13403.
[52] Y.J. Lu, et al., Liposomal ir-780 as a highly stable nanotheranostic agent for improved photothermal/photodynamic therapy of brain tumors by convection-enhanced delivery, Cancers 13 (15) (2021) (Basel).
[53] K.X. Vazquez-Prada, et al., A spiky silver-iron oxide nanoparticle for highly efficient targeted photothermal therapy and multimodal imaging of thrombosis, Small (2023) e2205744.
[54] M.L. Del Prado-Audelo, et al., *In vitro* cell uptake evaluation of curcumin-loaded PCL/F68 nanoparticles for potential application in neuronal diseases, J. Drug Deliv. Sci. Technol. 52 (2019) 905–914.
[55] A.U. Rehman, et al., Silver/iron oxide nano-popcorns for imaging and therapy, ACS Appl. Nano Mater. (2021).
[56] N.A. Fithri, et al., Gold-iron oxide nanoparticle: a unique multimodal theranostic approach for thrombosis, Appl. Mater. Today 31 (2023) 101750.
[57] B. Luzak, P. Siarkiewicz, M. Boncler, An evaluation of a new high-sensitivity PrestoBlue assay for measuring cell viability and drug cytotoxicity using EA.hy926 endothelial cells, Toxicol. Vitro 83 (2022) 105407.
[58] D.C. Arruda, et al., β-Actin-binding complementarity-determining region 2 of variable heavy chain from monoclonal antibody C7 induces apoptosis in several human tumor cells and is protective against metastatic melanoma, J. Biol. Chem. 287 (18) (2012) 14912–14922.
[59] W.T. Chan, et al., *In vivo* toxicologic study of larger silica nanoparticles in mice, Int. J. Nanomed. 12 (2017) 3421–3432.
[60] G.P. Otto, et al., Clinical chemistry reference intervals for C57BL/6J, C57BL/6N, and C3HeB/FeJ Mice (Mus musculus), J. Am. Assoc. Lab. Anim. Sci. 55 (4) (2016) 375–386.
[61] A. Houtmeyers, et al., Reference intervals for biochemical blood variables, packed cell volume, and body temperature in pet rats (Rattus norvegicus) using point-of-care testing, Vet. Clin. Pathol. 45 (4) (2016) 669–679.
[62] P.L. Michael, et al., Comprehensive evaluation of the toxicity and biosafety of plasma polymerized nanoparticles, Nanomaterials 11 (5) (2021) (Basel).
[63] M.A. Jarzabek, et al., Interrogation of gossypol therapy in glioblastoma implementing cell line and patient-derived tumour models, Br. J. Cancer 111 (12) (2014) 2275–2286.
[64] P. Ji, et al., Hyaluronic acid hydrophilic surface rehabilitating curcumin nanocrystals for targeted breast cancer treatment with prolonged biodistribution, Biomater. Sci. 8 (1) (2020) 462–472.
[65] A. Yuan, et al., Self-assembled PEG-IR-780-C13 micelle as a targeting, safe and highly-effective photothermal agent for *in vivo* imaging and cancer therapy, Biomaterials 51 (2015) 184–193.
[66] A. Cheung, et al., Targeting folate receptor alpha for cancer treatment, Oncotarget 7 (32) (2016) 52553–52574.
[67] M.Z.I. Khan, H.P. Štedul, N. Kurjaković, A pH-dependent colon-targeted oral drug delivery system using methacrylic acid copolymers. II. Manipulation of drug release using Eudragit® L100 and Eudragit S100 combinations, Drug Dev. Ind. Pharm. 26 (5) (2000) 549–554.
[68] M.K. Anwer, et al., Preparation, evaluation and bioavailability studies of eudragit coated PLGA nanoparticles for sustained release of eluxadoline for the treatment of irritable bowel syndrome, Front. Pharmacol. 8 (2017) 844.
[69] S. Luo, et al., IR780-loaded hyaluronic Acid@Gossypol–Fe(III)–EGCG infinite coordination polymer nanoparticles for highly efficient tumor photothermal/coordinated dual drugs synergistic therapy, Adv. Funct. Mater. 31 (24) (2021) 2100954.
[70] Y. Tian, et al., Dye-loaded mesoporous polydopamine nanoparticles for multimodal tumor theranostics with enhanced immunogenic cell death, J. Nanobiotechnol. 19 (1) (2021) 365.
[71] H. Zhu, et al., Laser-activated bioprobes with high photothermal conversion efficiency for sensitive photoacoustic/ultrasound imaging and photothermal sensing, ACS Appl. Mater. Interfaces 10 (35) (2018) 29251–29259.
[72] R. Ma, et al., Indocyanine green-based theranostic nanoplatform for NIR fluorescence image-guided chemo/photothermal therapy of cervical cancer, Int. J. Nanomed. 16 (2021) 4847–4861.
[73] Z. Jiang, et al., Zoledronate and SPIO dual-targeting nanoparticles loaded with ICG for photothermal therapy of breast cancer tibial metastasis, Sci. Rep. 10 (1) (2020) 13675.
[74] S. Roberts, et al., Sonophore-enhanced nanoemulsions for optoacoustic imaging of cancer, Chem. Sci. 9 (25) (2018) 5646–5657.
[75] J.A. Ledermann, S. Canevari, T. Thigpen, Targeting the folate receptor: diagnostic and therapeutic approaches to personalize cancer treatments, Ann. Oncol. 26 (10) (2015) 2034–2043.
[76] N. Viola-Villegas, A. Vortherms, R.P. Doyle, Targeting gallium to cancer cells through the folate receptor, Drug Target Insights 3 (2008) DTI.S651.
[77] B.A. Kamen, et al., Farletuzumab, a monoclonal antibody against folate receptor alpha (FRα), does not block folate or anti-folate binding or alter drug potency assessed *in vitro*, J. Clin. Oncol. 29 (15_suppl) (2011) p. e13544-e13544.
[78] H. Cao, et al., Albumin biomimetic nanocorona improves tumor targeting and penetration for synergistic therapy of metastatic breast cancer, Adv. Funct. Mater. 27 (11) (2017) 1605679.
[79] H.D.N. Tran, et al., Influence of nanoparticles on the haemostatic balance: between thrombosis and haemorrhage, Biomater. Sci. 10 (1) (2022) 10–50.
[80] M. Weber, et al., Blood-contacting biomaterials: in vitro evaluation of the hemocompatibility, Front. Bioeng. Biotechnol. 6 (2018) 99.
[81] L. Wang, et al., Sequential targeting biomimetic nano platform for enhanced mild photothermal therapy and chemotherapy of tumor, Comput. Struct. Biotechnol. J. 21 (2023) 2780–2791.

[82] K. Wang, et al., Self-assembled IR780-loaded transferrin nanoparticles as an imaging, targeting and PDT/PTT agent for cancer therapy, Sci. Rep. 6 (1) (2016) 27421.
[83] Y.N. Zhang, et al., Nanoparticle-liver interactions: cellular uptake and hepatobiliary elimination, J. Control. Release 240 (2016) 332–348.
[84] A. Taruttis, V. Ntziachristos, Advances in real-time multispectral optoacoustic imaging and its applications, Nat. Photonics 9 (4) (2015) 219–227.
[85] J. Hong, et al., High drug payload curcumin nanosuspensions stabilized by mPEG-DSPE and SPC: *in vitro* and *in vivo* evaluation, Drug Deliv. 24 (1) (2017) 109–120.

Supporting Information for

Polysuccinimide-based Nanoparticle: A Nanocarrier with Drug Release Delay and Zero Burst Release Properties for Effective Theranostics of Cancer

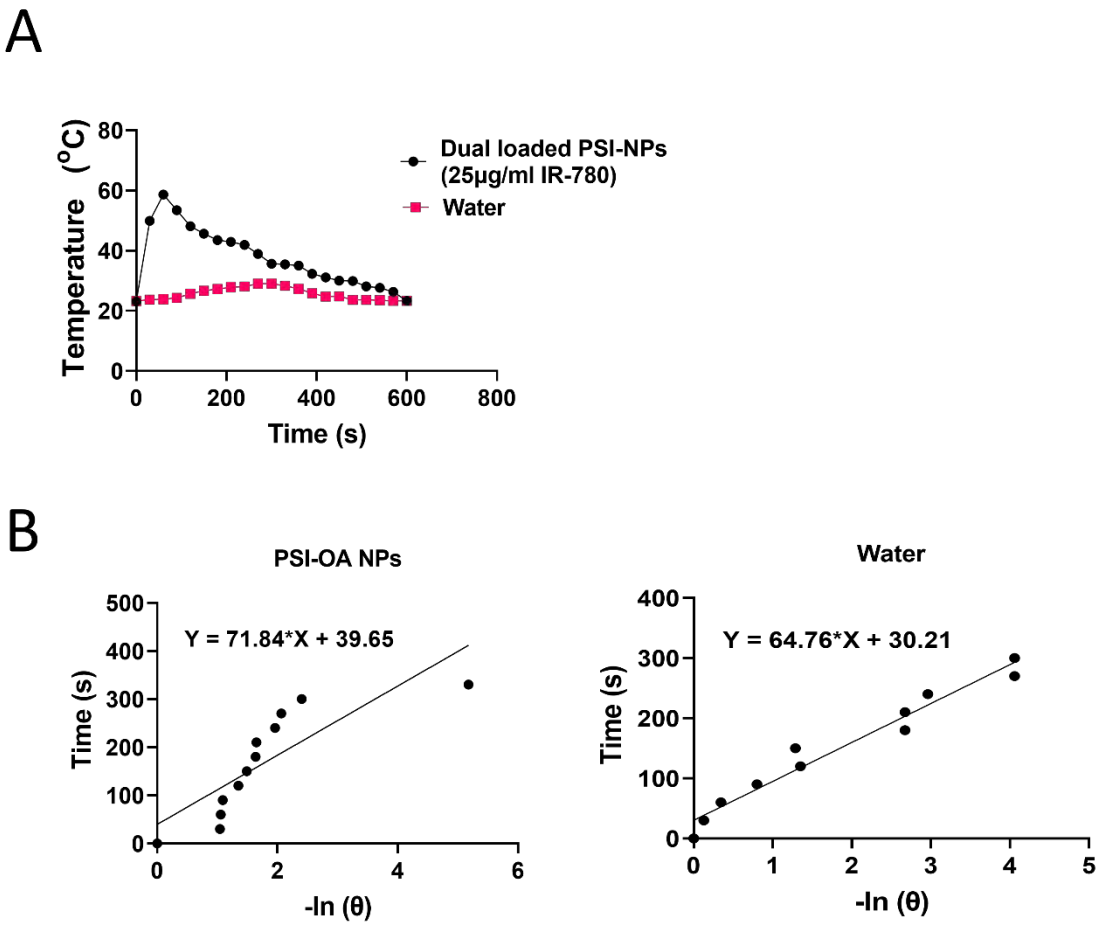

Figure S1. Photothermal conversion efficiency calculation. **A)** Temperature change at every 30 seconds for 300 seconds of PSI-OA NPs (25 µg/ml) and water with NIR irradiation (808 nm, 2 W/cm^2). At the end of 300 seconds, the laser was shut off and temperature change was recorded for a further 300 seconds. **B)** Plot of -ln(Θ) vs time of the cooling period to calculate the photothermal conversion efficiency.

Photothermal conversion efficiency was calculated based on Qian et al [1] with the application of **Equation 1** as detailed below:

$$\eta = \frac{hs\,(T_{max} - T_{surr}) - Q_{Dis}}{I(1 - 10^{-A_{808}})} \qquad \text{Equation 1}$$

h = heat transfer coefficient
s = surface area of the container
Tmax = maximum temperature obtained with laser irradiation
Tsurr = initial temperature before the laser irradiation
Q_{Dis} = heat absorbed by solvent and container

I = Intensity of the laser
A_{808} = Absorbance of NPs at 808 nm

hs value was obtained via a dimensionless parameter Θ and a sample system time constant which can be calculated by the following **Equation 2** and **3** respectively:

$$\Theta = \frac{T - T_{surr}}{T_{Max} - T_{Surr}} \quad \text{Equation 2}$$

$$t = -\tau_s \, ln\,(\Theta) \quad \text{Equation 3}$$

where $\boldsymbol{\tau}$s can be determined by obtaining the slope value of -ln(Θ) vs time (Figure S1B) from the cooling period of the observation. Based on this, we obtained $\boldsymbol{\tau}$s value for PSI-OA NPs and water as 71.84 and 64.76 respectively.

Subsequently, hs is obtained with Equation 4:

$$hs = \frac{m\,C}{\tau_s} \quad \text{Equation 4}$$

m = 0.1 g

C = 4.2 J/g°C.

Hence, hs value is calculated to be 0.0058 W/°C, (T_{max} - T_{surr}) = 35.5 °C, Q_{Dis}= 0.0065 W/°C, laser power = 0.64 W, Absorbance at 808 nm = 2.1 are substituted into **Equation 1** to obtain a photothermal conversion efficiency of **31.5** %.

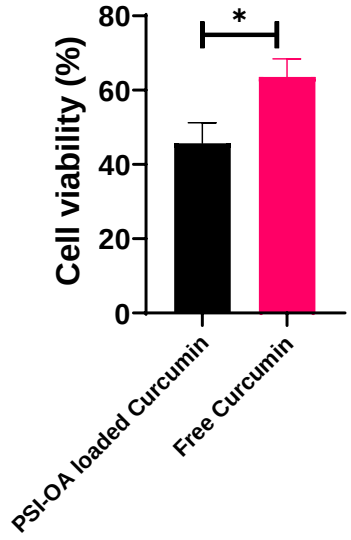

Figure S2: Cytotoxicity of Curcumin. U87 MG cells were treated with PSI-OA NPs loaded with Curcumin and free Curcumin for 12 h (18.3 µg/mL of Curcumin). * Compared to free Curcumin. * $p < 0.05$.

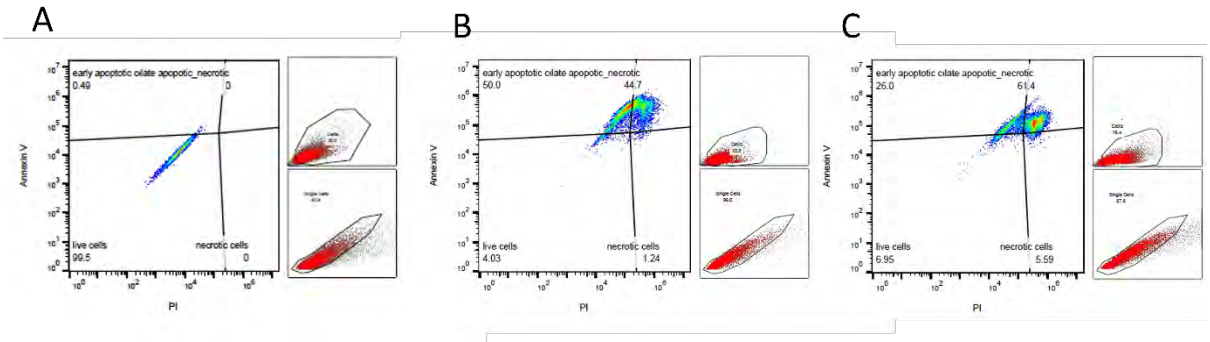

Figure S3. Flow cytometry analysis of U87MG cells to determine different population of apoptotic cells. a) untreated control, b) treated with 25 µg/ml of FA conjugated dual loaded PSI-OA NPs. c) NPs and laser irradiation at 2W/cm^2, 5 mins.

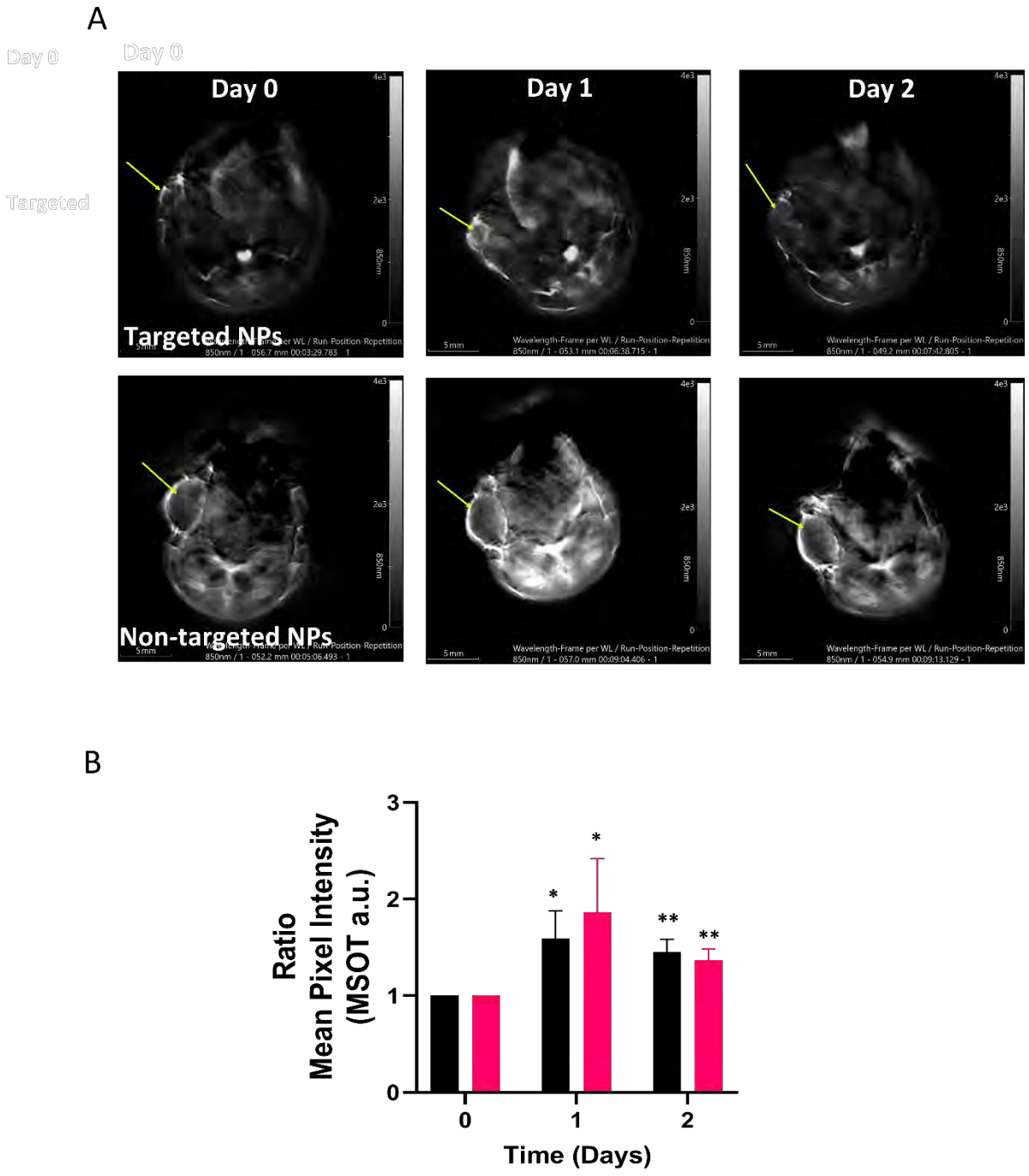

Figure S4. MSOT imaging. A) Representative MSOT image frames of the tumour centre captured at day 0, 1, and 2 for each group. B) Quantitative ratiometric analysis at 780 nm from the centre tumours injected with PSI-OA and FA-PSI-OA. * Compared with pre injection at Day 0. * $p < 0.05$, ** $p < 0.01$. n = 3.

Table S1. Characterisation of NPs.

Sample	Size (nm)	PDI	Zeta Potential in DI water (mV)
PSI-OA NPs	181.0	0.135	-29.8
PSI-OA-IR 780	199.3	0.156	-30.1
PSI-OA-Curcumin	201.3	0.148	-28.3
PSI-OA-Curcumin & IR780	211.1	0.149	-35.6
FA-PSI-OA-Curcumin & IR780	220.0	0.181	-20.6

Table S2. Different mass ratio of FA-PEG-NH_2 conjugation to PSI-OA dual loaded NPs.

Sample (Dual loaded)	Size (nm)	PDI	Zeta potential in DI water (mV)
PSI-OA NPs	211.1	0.149	-35.6
FA:NP 1:10	220	0.181	-20.6
FA:NP 1:5	245	0.35	-30
FA:NP 1:2	238	0.37	-32